Chapter 1

Functional MRI Data and Brain Parcellation

Paragraph 1: Write here what would happen in the ideal world
Paragraph 2: Write here why we cannot reach this ideal easily
Paragraph 3: Write here what we do instead to overcome this problem

1.1 fMRI Background

Functional magnetic resonance imaging (fMRI) is a technique that measures brain activity by detecting the blood flow and oxygenation levels in different parts of the brain. When an area of the brain is in use, it consumes more oxygen and hence requires more blood. The fMRI machine measures the strength of magnetic signals from the hydrogen atoms of water molecules in blood. The signal emitted depends on the contents of the blood, in particular how much oxygen it contains. This detection method is referred to as blood-oxygen-level dependent, or BOLD.

The fMRI machine detects, for all regions of the brain, the change in magnetic signal within a given time frame (typically 2 seconds) and records this as a 3-dimensional image. This image is comprised of units called voxels, each representing a cube of brain tissue. These 3-D units are analogous to 2-D pixels that make up computer screens. Each voxel represent around a million brain cells.

This measurement made repeatedly over all 2 second intervals in the course of around 10 minutes. The resulting data collected is a time series of

3-D images.

1.2 Parcellation Background

A fundamental goal of neuroscience is to understand the functional connectivity of the brain. Functional connectivity refers to the set of statistical dependencies between the activity levels of different regions of the brain. Numerous studies have highlighted the linkage of certain brain regions with motor, language, and memory tasks. They have shown functional connectivity to be heavily dependent on what actions the subject is performing, the physiological qualities of the subject, and even the timescale over which the data is collected.

Consequently, neuroscientists developed and focused on the idea of resting-state functional connectivity. The observation behind this approach is that the brain exhibits some regular patterns of functional organization even when the subject is resting and not actively engaged in a task. (The subject may be daydreaming or mind-wandering.) The goal of establishing a map of resting-state functional connectivity thus emerged as a refinement to the goal of understanding the baseline organization of the brain.

In recent years neuroscientists have increasingly viewed the analysis of functional connectivity through the lens of graph theory. The brain was modeled as a graph with vertices representing fMRI voxels and edges representing connections between voxels with weights defined by some measure of statistical dependency.

The problem with this framework is that the sheer size, complexity, and detail of the voxel graphs, coupled with the variation in brain structure between individuals, made it too difficult to draw scientific conclusions from them. A coarser map was needed, one that ideally would retain the most useful information in the voxel-level graphs.

Hence the idea of parcellation emerged. Brain parcellation roughly means the task of grouping spatially-adjacent voxels so as to maximize the statistical dependence of signals arising from voxels in the same group. Early attempts at parcellation were focused on brain anatomy. For instance the popular Automatic Anatomic Labeling atlas (AAL) [Tzourio-Mazoyer et al., 2002] defines 116 parcels based on the similarity of brain tissue and other structural information. Many findings based on this parcellation have been published [Hartman et al., 2011, He et al., 2009, Liu et al., 2008, Lynall et al., 2010, Power et al., 2011,

Salvador et al., 2005, Spoormaker et al., 2010, Supekar et al., 2008, Tian et al., 2011, Wang et al., 2009]. However, the AAL parcellation suffers two major shortfalls. First, it is not based on statistical dependence. Second, it cannot adapt to accomodate researchers who want more than 116 parcels and a higher-resolution network. The answer to these issues lies in data-driven parcellations based on functional connectivity.

The bulk of data-driven parcellations in the literature are based on spatially-constrained clustering methods that relate to some approximate measure of statistical dependency such as Pearson correlation. To list a few, [Biswal et al., 2010, Smith et al., 2009] and [Chen et al., 2008] use Independent Component Analysis and Principal Components Analysis. [Beckmann et al., 2005, De Luca et al., 2006] and [Ryali et al., 2013] builds a mixture model for how the voxel signals is generated and cluster using an Expectation-Maximization algorithm.

Another large body of work uses K-means clustering [Flandin et al., 2002, Mezer et al., 2009, Peltier et al., 2003, Thirion et al., 2006] with some spatial contraints imposed to ensure connectivity. Hierarchical clustering methods used in [Diez et al., 2014, Bellec et al., 2006, Lu et al., 2003, Heller et al., 2006, Blumensath et al., 2013, **?**] have the advantage of naturally producing connected parcels.

Spectral methods make up another large body of literature on voxel clustering [Craddock et al., 2012, Van Den Heuvel et al., 2008, Shen et al., 2010, Newman, 2006, Shen et al., 2013, Zhang et al., 2014]. These methods, which use the eigenvectors of the graph Laplacian matrix, are characterized by the choice of edge weights (either Pearson's correlation or Gaussian kernel) and the choice of cut objective (usually normalized cut) and can be either recursive or multiway. For details on these methods, see Chapter 5.

There is a wide literature of less commonly-used methods. [Alexander-Bloch et al., 2012] uses a method based on normalized mutual information. [Cohen et al., 2008, Gordon et al., 2014, Barnes et al., 2011] adapt edge-detection algorithms for planar graphs from computer vision.

1.3 Overall Strategy

We continue in the tradition established by the aforementioned authors of framing the problem of brain parcellation as a problem of graph partitioning. Our contribution to this field is four-part:

1. We introduce the usage of a fairly new statistic for measuring depen-

dency: distance correlation. Unlike traditional statistics such as Pearson's correlation, distance correlation has the special property that it is 0 if and only if the two random variables are independent. This brings brain parcellation back to framework of mapping functional connectivity defined as statistical dependence of voxel actvity.

2. We introduce the novel graph partitioning objective of Maximize Average Within-Edge (MAWE) and justify its usage in conjunction with distance correlation. We also develop metrics for evaluating the smoothness and size balance of parcellations.

3. We propose a number of methods, some original and some borrowed, for approximately solving the graph partitioning problem of MAWE with constraints on parcel smoothness and size.

4. We carry out these methods on fMRI data collected from patients with and without autism spectrum disorder.

1.4 About the Data

Autism spectrum disorders (ASD) represent a formidable challenge for psychiatry and neuroscience because of their high prevalence, lifelong nature, complexity and substantial heterogeneity. Roughly 1% of children worldwide are diagnosed with ASD [Centers for Disease Control, 2010]. We obtained data for our parcellation problem from the Autism Brain Imaging Data Exchange (ABIDE) – a consortium that has collected 1112 resting-state fMRI data sets collected from 539 individuals with ASDs and 573 age-matched typical controls.

For simplicity in this thesis, we focus on 6 autistic and 6 control subjects scanned at the University of Pittsburgh School of Medicine. The autistic subjects included individuals from 7 to 35 years of age, with a well-characterized Autistic Disorder. Patients were diagnosed with the Autism Diagnostic Interview-Revised [Lord et al., 1994] and the Autism Diagnostic Observation Schedule-General [Lord et al., 2000], under expert clinical opinion. Typical controls were healthy individuals, with no history of head trauma, birth complications, seizures, or psychiatric disorder. The controls were also matched by age, full-scale IQ, and gender with patients in the ASD group. For more information, refer to `http://fcon_1000.projects.nitrc.org/indi/abide/`.

In order to register each subject's brain to a common brain space, we use the Montreal Neurological Institute's (MNI) standardized brain [Evans et al., 1993, Collins et al., 1994]. The MNI standardized brain template MNI152 was taken from the average of 152 normal MRI scans. We use the unsymmetrical MRI scan with voxels corresponding to cubes with an edge-length of 2 millimeters. The dimensions of this MNI152 template are $91 \times 109 \times 91$ voxels with 228,453 voxels representing space occupied by the brain.

We preprocessed the raw data from ABIDE using the Configurable Pipeline for the Analysis of Connectomes (C-PAC) alpha version 0.3.9. C-PAC is an open-source software pipeline for automated preprocessing and analysis of resting-state fMRI data. The image preprocessing steps included slice-timing and motion correction, nuisance signal regression and temporal filtering. The derived resting-state fMRI data were normalized to the MNI152 template.

Following C-PAC preprocessing, we converted the 4-dimensional fMRI data (a 3-dimensional image varying with time) to a 2-dimensional matrix with each column representing a different voxel and each row a time sample. Since C-PAC removed most autocorrelations in the data, we can reasonably treat each row observation as independently from the same unknown distribution.

1.5 Chapter Summaries

Chapter 2 presents the theory of distance correlation, which belongs to the larger family of energy statistics. We argue for using distance correlation as a better alternative to Pearson's in problems of dependence-based clustering.

Chapter 3 defines the set of valid parcellations and introduces validation criteria for measuring how well a parcellation captures functional connectivity. The validation criteria are based on distance correlation. In particular, we introduce the objective of Maximize Average Within-Edge (MAWE) that serves as the primary measure of statistical dependency within parcels throughout this thesis. Additionally, the chapter presents metrics for quantifying size balance, smoothness, and similarity of two parcellations.

Chapter 4 details the first class of parcellation methods that are based on graph-growing heuristics. In particular, we introduce a new data structure called the Contractible Graph and its associated algorithm Edge-Contract. We illustrate the efficient implementation of Edge-Contract and show that it can be flexibly extended to encourage parcellations that are smooth and

size-balanced.

Chapter 5 explores the well-established spectral methods for graph partitioning, beginning with an exposition on the early bipartitioning method and then moving on to its more sophisticated multiway version that minimizes the ratio-cut of a partitioning and requires K-means.

Chapter 6 begins with a very recently developed clustering method based on a symmetric factorization of the adjacency matrix into nonnegative matrices and illustrates the connection between this and spectral multiway partitioning. The second half discusses the case of 0-1 symmetric matrix factorization and presents two original approaches.

Chapter 7 presents two novel formulations of a connectivity-relaxed version of MAWE as a generalized 0-1 fractional program which has an equivalent mixed integer linear program. In particular, we derive both a globally optimal formulation and an more efficient approximate one.

Chapter 8 compares all of the aforementioned parcellation methods and presents the parcellation results of some of them on the ABIDE fMRI data.

Chapter 2

Energy Statistics

In this section, we discuss distance correlation, their benefits and their mathematical properties. Distance correlations first appeared in [Székely et al., 2007] but has seen made multiple appearances in other papers stating various extensions and applications. The two followup papers that contain a thorough survey of these extensions are in [Székely and Rizzo, 2013] and [Sejdinovic et al., 2013].

As we will see, the distance correlation is a non-linear measurement of the dependency between two distributions, and it equals zero if and only if the two distributions are independent of one another. This measurement will be used to determine which spatially-adjacent voxels are related and serves as the statistical foundation of our parcellation procedures. While many works have gone ahead to use distance correlation to test the null hypothesis that two distributions are independent, we simply use the distance correlation as a statistical guide to aid our graph-based algorithms generate a reasonable parcellation.

2.1 Benefits of Distance Correlation

To measure dependence, statisticians have traditionally used the Pearson correlation coefficient, in addition to the rank-based Kendall tau and Spearman rho. These statistics work well when the underlying relationship between the two random variables is linear, in the case of Pearson, or can be linear after a monotonic transformation, in the case of Kendall and Spearman. Due to their restrictions, these correlation coefficients will fail to capture many kinds of dependency relationships. The figure below illustrates several instances of

pairs of random variables whose depencency structure is not detected by the three correlation coefficients.

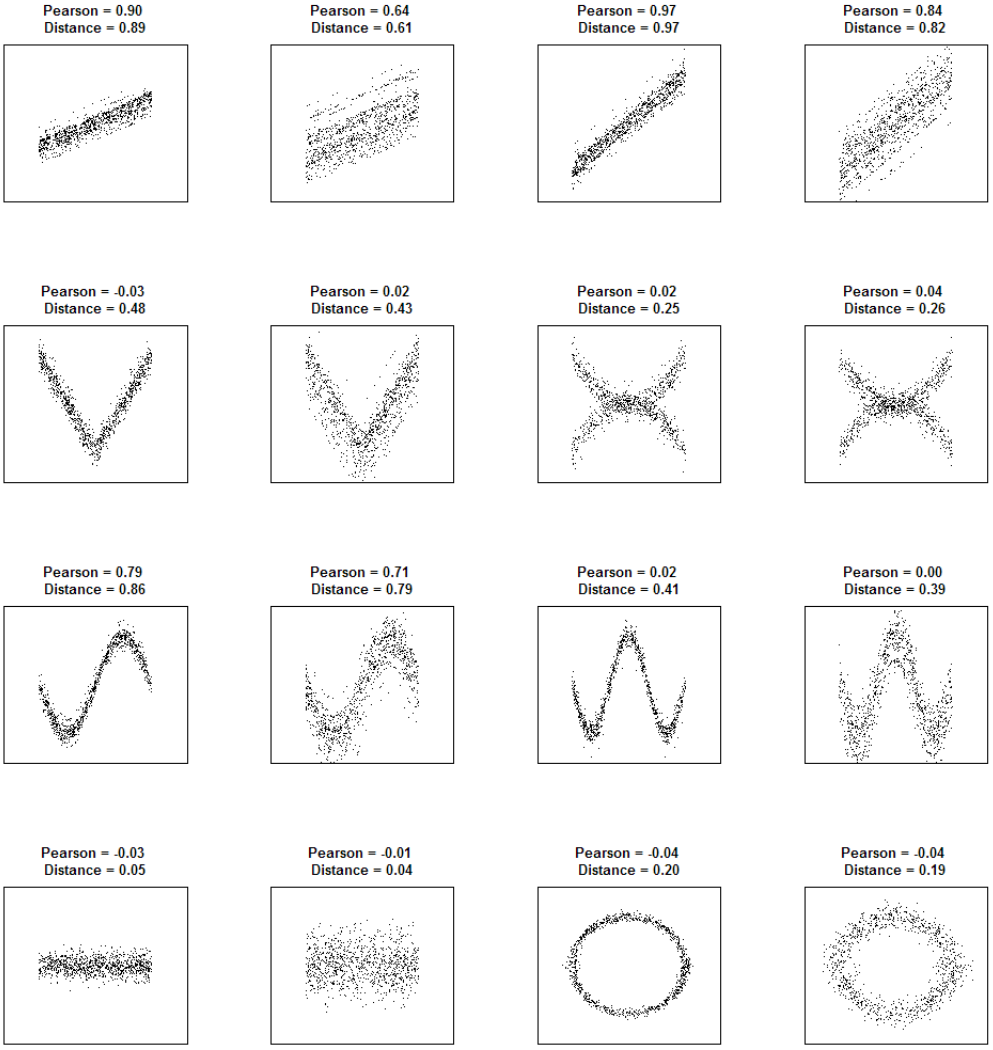

Non-linear dependency relationships also exist in the ABIDE 50002 fMRI data. The scatterplots below show time samples of spatially adjacent voxels. These instances were found by searching for the maximum difference in rank of energy distance correlation and the coefficient of determination, or Pearson squared.

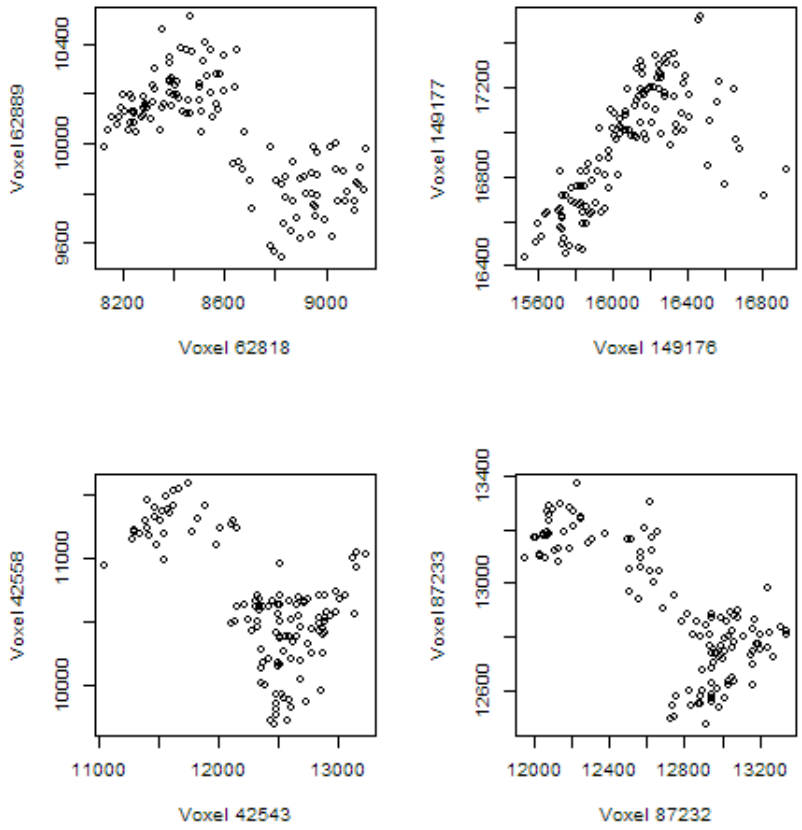

2.2 Distance Covariance

We first discuss the definition of distance covariance, from which the definition of distance correlation will naturally follow. We first start with the population quantity where $\mathcal{V}^2(X, Y)$ represents the population distance covariance between two distributions, one over the random variable X in a p-dimensional space and the other over Y in a q-dimensional space. In our application, $p = q$. Let φ_X denote the characteristic function associated with the density of X. For some positive weight function $w : \mathbb{R}^p \times \mathbb{R}^q \mapsto [0, \infty)$ define the norm $\|\cdot\|_w : \{\gamma : \mathbb{R}^p \times \mathbb{R}^q \mapsto \mathbb{C}\} \mapsto [0, \infty)$ as

$$\|\gamma\|_w^2 = \int_{\mathbb{R}^{p+q}} |\gamma(s,t)|^2 w(s,t) ds dt.$$

In the case where the subscript w is omitted, it is implied that $w = 1$, the constant function taking value one. Hence $\|\cdot\|^2$ is the typical definition of the ℓ_2 (Euclidean) norm squared.

Definition 2.2.1 (Distance covariance) *Let X and Y be two d-dimensional random vectors with $\mathbf{E}\|X\| + \mathbf{E}\|Y\| < \infty$. Their distance covariance is*

$$\begin{aligned}\mathcal{V}^2(X,Y) &= \|\varphi_{X,Y}(s,t) - \varphi_X(s)\varphi_Y(t)\|_w^2 \\ &= \int_{\mathbb{R}^{p+q}} \frac{|\varphi_{X,Y}(s,t) - \varphi_X(s)\varphi_Y(t)|^2}{\|s\|^{1+p}\|t\|^{1+q}} dsdt\end{aligned}$$

where $w(s,t) = \dfrac{1}{\|s\|^{1+p}\|t\|^{1+q}}$.

It is clear that $\mathcal{V}^2(X,Y) = 0$ if and only if $X \perp\!\!\!\perp Y$. To explicitly see why this is called a distance *covariance*, we notice that the definition of $\mathcal{V}^2(X,Y)$ can be rewritten in terms of covariances. Let X, X', X'' be three independent copies of the same random variable but drawn from the same distribution.

Proposition 2.2.2 ([Székely, 2003] (Theorem 1))

$$\begin{aligned}\mathcal{V}^2(X,Y) &= \mathbf{E}[\|X - X'\|\|Y - Y'\|] + \mathbf{E}[\|X - X'\|]\mathbf{E}[\|Y - Y'\|] - 2\mathbf{E}[\|X - X'\|\|Y - Y''\|] \\ &= \mathrm{Cov}(\|X - X'\|, \|Y - Y'\|) - 2\mathrm{Cov}(\|X - X'\|, \|Y - Y''\|)\end{aligned}$$

With a slight overload of notation, we define the distance variance to be the distance covariance between the same variable.

Definition 2.2.3 (Distance variance)

$$\mathcal{V}^2(X) = \mathcal{V}^2(X,X)$$

Using the standard relationship between covariance and correlation, we define the distance correlation as such. It is clear from the definition that this quantity is bounded between ± 1, much like the Pearson correlation.

Definition 2.2.4 (Distance correlation)

$$\mathcal{R}^2(X,Y) = \frac{\mathcal{V}^2(X,Y)}{\mathcal{V}(X)\mathcal{V}(Y)}$$

The above definitions all hold for the population quantities, but now we are interested in estimating them. While the population distance covariance (and the population distance correlation) are equal to 0 if and only if the two distributions are independent, we hope to estimate a sample distance correlation which is close but not necessarily 0 when the two distributions are independent.

For independent, identically-distributed sample $\{(X_i, Y_i)\}_{i=1}^n$, let $\widehat{\varphi}_X(t) = \frac{1}{n}\sum_{i=1}^n \exp(it^T X_i)$ be the empirical characteristic function for X and likewise for Y. An estimate of $\mathcal{V}^2(X,Y)$ replaces the unknown characteristic functions with the empirical characteristic functions. Thanks to Proposition 2.2.2, we will simply replace the expectations by the same averages.

Definition 2.2.5 (Sample Distance Covariance)

$$\widehat{\mathcal{V}}^2(X,Y) \equiv \|\widehat{\varphi}_{X,Y}(s,t) - \widehat{\varphi}(s)\widehat{\varphi}_Y(t)\|_w^2 = S_1 + S_2 - 2S_3$$

where

$$\begin{aligned}
S_1 &= \frac{1}{n^2}\sum_{k=1}^n\sum_{l=1}^n \|X_k - X_l\|\|Y_k - Y_l\| \\
S_2 &= \left(\frac{1}{n^2}\sum_{k=1}^n\sum_{l=1}^n \|X_k - X_l\|\right)\frac{1}{n^2}\sum_{k=1}^n\sum_{l=1}^n \|Y_k - Y_l\| \\
S_3 &= \frac{1}{n^3}\sum_{k=1}^n\sum_{l=1}^n\sum_{m=1}^n \|X_k - X_l\|\|Y_k - Y_m\|
\end{aligned}$$

Alternatively, we can let $A, B \in \mathbb{R}^{n\times n}$ such that $A_{kl} = \|X_k - X_l\|$ and $B_{kl} = \|Y_k - Y_l\|$ (A and B are symmetric elementwise nonnegative). Let $\overline{X} = \frac{1}{n^2}\sum_{k,l=1}^n X_{kl}$. Then

$$\widehat{\mathcal{V}}^2(X,Y) = \overline{A \circ B} + \overline{A}\cdot\overline{B} - \frac{2}{n}(\overline{AB})$$

where $\circ$ means element-wise multiplication.

Estimates of distance variance and distance correlation are defined analogously.

2.3 Statistical Review

We now review some key properties that relate the sample distance covariance to the population distance covariance that helps give insight. We simply state the theorems and refer to the papers for interested readers.

First, we relate the distance correlation to Pearson correlation.

Definition 2.3.1 (α-distance covariance) *For* $0 < \alpha < 2$

$$\mathcal{V}_\alpha^2(X,Y) = \frac{1}{C(p,\alpha)C(q,\alpha)} \int_{\mathbb{R}^{p+q}} \frac{|\varphi_{X,Y}(s,t) - \varphi_X(s)\varphi_Y(t)|^2}{\|s\|^{\alpha+p}\|t\|^{\alpha+q}} dsdt$$

Proposition 2.3.2 ([Székely and Rizzo, 2013] (Section 7.2)) *If* $\mathbf{E}[\|X\|^\alpha] + \mathbf{E}[\|Y\|^\alpha] < \infty$ *then*

$$\mathcal{V}_\alpha^2(X,Y) = \mathbf{E}[\|X-X'\|^\alpha\|Y-Y'\|^\alpha] + \mathbf{E}\|X-X'\|^\alpha \mathbf{E}\|Y-Y'\|^\alpha - 2\mathbf{E}[\|X-X'\|^\alpha\|Y-Y''\|^\alpha]$$

In particular, if $\alpha = 2$, $p = q = 1$, *the distance correlation is the absolute value of Pearson's correlation coefficient.*

Next, we show statement ensuring consistency under the existence of the first moments.

Proposition 2.3.3 ([Székely et al., 2007] (Corollary 1)) *If* $\mathbb{E}(\|X\| + \|Y\|) < \infty$, *then almost surely*

$$\lim_{n\to\infty} \widehat{\mathcal{R}}(X,Y) = \mathcal{R}(X,Y)$$

While we did not find a theorem explicitly stating the rate of convergence, the above theorem gives us satisfaction that if $\mathcal{V}(X,Y) = 0$ (meaning X and Y are independent), then as long as we have enough samples, $\widehat{\mathcal{V}}(X,Y)$ will approach 0. In our case, n refers to the number of time samples which typically range from $n = 100$ to $n = 200$.

We next show the asymptotic distribution of the sample distance covariance under independence of X and Y. While this is not used in our work (as we do not apply the hypothesis test), this can inspire future work where instead of computing the sample energy statistics $\widehat{\mathcal{V}}(X,Y)$, we compute the p-value under the null hypothesis $H_0 : X \perp\!\!\!\perp Y$.

To formulate the asymptotic distribution, we need additional notation. Let Q be a random variable where

$$Q \stackrel{D}{=} \sum_{j=1}^{\infty} \lambda_j Z_j^2,$$

where Z_j are independent, standard normal random variables and $\{\lambda_j\}$'s are nonnegative constants dependent on the characteristic functions on the joint distribution (X, Y) such that $\mathbb{E}[Q] = 1$. Here, we put the superscript D to denote equality in distribution.

Proposition 2.3.4 ([Székely et al., 2007] (Corollary 2)) *If* $\mathbb{E}(\|X\|+\|Y\|) < \infty$, *then*

- *If* X *and* Y *are independent, then* $n\widehat{\mathcal{V}}^2/S_2 \stackrel{D}{\to} Q$.
- *If* X *and* Y *are dependent, then* $n\widehat{\mathcal{V}}^2/S_2 \stackrel{P}{\to} \infty$.

Here, the superscript D and P denote convergence in distribution and probability as n goes to infinity. More explicit asymptotic distributions are given in [Székely and Rizzo, 2013] when X and Y are Gaussian, but in general, bootstrapping procedures can be used to test this hypothesis. Similar procedures can be derived on the distance correlation.

In all our computations throughout our thesis, we use the `dcor` function in the `energy` package to compute the distance correlation efficiently.

Chapter 3

Criteria for Evaluating Parcellations

In chapter one we discussed our graphical approach to the brain parcellation problem. We construct a weighted undirected graph where each vertex is a voxel. The graph reflects the spatial position of the voxels; it connects each vertex to the vertices representing the voxel's six cubically adjacent neighbors. The weights on these edges are sample distance correlation statistics between the adjacent voxels in the time series and they measure statistical dependence, with 0 denoting full independence and 1 full dependence. Let $G(V, E)$ denote this graph, its vertices, and its edges.

In this context, a valid k-fold partition $\mathcal{P}_k$ of the graph G is a collection of vertex subsets $(V_1, ..., V_k)$ satisfying the following:

1. $V_i \neq \varnothing$ for all $V_i \in \mathcal{P}_k$
2. $\bigcup_{i=1}^{k} V_i = V$
3. $V_i \cap V_j = \varnothing$ for all $V_i, V_j \in \mathcal{P}_k$
4. V_i is connected (i.e. for every two vertices in V_i, there is a path between them) for all $V_i \in \mathcal{P}_k$

In this chapter we will suggest various criteria for measuring the goodness-of-fit of partitions and discuss their statistical and computational advantages and drawbacks.

3.1 Within-Parcel Similarity

Voxels in the same parcel are ideally highly dependent on one another in the time series of fMRI data. As discussed in the previous chapter, distance correlation is a good measure of dependence. The distance correlation between two random vectors equals zero if and only if the two random vectors are independent, which is not true of correlation statistics such as Pearson's.

Let $\mathcal{R}(x, y)$ denote the distance correlation between two voxels x and y. Let V and W be any parcels. We will use E_V to denote the set of edges with one end in V and one end not in V, and $E_{V,W}$ the set of edges with one end in V and one in W. Mention if we want to maximize or minimize these criteria. Do it for each of them

Definition 3.1.1 (Within-Score)

$$\frac{1}{k} \sum_{V \in \mathcal{P}_k} \frac{1}{|V|^2} \sum_{x,y \in V} \mathcal{R}(x, y)$$

The Within-Score is non-spatial; it considers all pairs of voxels equally regardless of whether they are adjacent. As a result, it is a good measure of how much the voxels within each parcel are dependent on each other as a set. The downside of this criterion is that it is very expensive to compute. With over 300,000 voxels in an fMRI data set we would potentially have to compute tens of billions of distance correlation statistics, each of which takes time proportional to the number of samples squared.

An alternative and far less expensive criterion that measures within- parcel similarity works by counting distance correlations between adjacent pairs of voxels.

Definition 3.1.2 (Adjacent-Score)

$$\frac{1}{k} \sum_{V \in \mathcal{P}_k} \frac{1}{|E_{V,V}|} \sum_{(x,y) \in E_{V,V}} \mathcal{R}(x, y)$$

Rather than treat parcels as sets with no spatial information, the Adjacent-Score does the opposite by only considering the pairwise dependency of adjacent voxels. For sparse graphs such as ours, the number of distance correlation computations is proportional to the number of vertices.

An intermediate possibility we did not explore is to consider all pairs of voxels up to some maximum spatial distance from each other and perform a weighted averaging of sample pairwise distance correlations, with weights that depend on spatial distance.

3.2 Between-Parcel Dissimilarity

To evaluate parcellation quality, it is also useful to measure how dependent voxels belonging to different parcels are on each other. To this end we define two criterion similar to the Within-Parcel criterion; a non-spatial metric called the Between-Score and its spatial metric the Boundary-Score.

Definition 3.2.1 (Between-Score)

$$\frac{1}{\binom{k}{2}} \sum_{V,W \in \mathcal{P}_k, V \neq W} \frac{1}{|V||W|} \sum_{x \in V, y \in W} \mathcal{R}(x, y)$$

Definition 3.2.2 (Boundary-Score)

$$\frac{1}{\binom{k}{2}} \sum_{V,W \in \mathcal{P}_k, V \neq W} \frac{1}{|V||W|} \sum_{(x,y) \in E_{V,W}} \mathcal{R}(x, y)$$

Generally both of these quantities are more expensive to compute than their Within-Parcel counterparts. Boundary-Score is easy enough to compute for validation purposes, but does not convey much additional information beyond what the Adjacency-Score does, in the sense that the edges used in the computation of Adjacency-Score are the complement of the edges used in the Boundary-Score.

The ability of distance correlation to generalize to pairs of random vectors of arbitrary dimension gives us another way of computing the dependency between two parcels. The Multivariate Between-Score defined below treats parcels as random vectors and computes the distance correlation at the parcel level rather than voxel level. The result is a measure of non-spatial between-parcel similarity that is also computationally feasible. For this reason we will use Multivariate Between-Score as our primary measure of parcel dissimilarity.

Definition 3.2.3 (Multivariate Between-Score)

$$\frac{1}{\binom{k}{2}} \sum_{V,W \in \mathcal{P}_k, V \neq W} \mathcal{R}(V, W)$$

3.3 Graph Cuts

Closely related to the Boundary-Score is the notion of a graph cut from computer science. A *cut set* is the set of edges with endpoints in different parcels. The *cut weight* is the sum of weights of all edges in the cut set and can be expressed as

$$\frac{1}{2}\sum_{V\in\mathcal{P}_k}\sum_{x,y\in E_V}\mathcal{R}(x,y)$$

The *ratio cut* defined below is a weighted version of the cut weight:

$$\frac{1}{2}\sum_{V\in\mathcal{P}_k}\frac{1}{|V|}\sum_{x,y\in E_V}\mathcal{R}(x,y)$$

The subfield of graph partitioning is concerned with minimizing cut weight, ratio cut, and several other related quantities. Over the last several decades a number of highly effective approximation algorithms have been developed to find partitions of graphs that minimize these quantities. Later chapters will explore how these methods work for brain parcellation.

3.4 Balance and Jaggedness

In addition to the above distance correlation based criteria, there are two additional metrics concerned with parcel shape.

Definition 3.4.1 (Balance)

$$\frac{1}{k}\frac{1}{\max_{V\in\mathcal{P}_k}|V|}\sum_{V\in\mathcal{P}_k}|V|$$

The Balance-Score ranges from 1 (all equally sized parcels) to 0 (two parcels with one of size zero).

Definition 3.4.2 (Jaggedness)

$$\frac{1}{k}\sum_{V\in\mathcal{P}_k}\frac{|E_V|^{\frac{3}{2}}}{|V|}$$

The $\frac{3}{2}$ power makes the ratio invariant on parcel size. Not a fan of this sentence about ratio invariant. Maybe just say it's used to account for the fact that numerator is a surface area-like measurement while the denominator is a volume-like measurement. For instance, a $n \times n \times n$ cube of vertices would have a jaggedness of $6^{\frac{3}{2}}$ which does not depend on n.

3.5 Comparing Multiple Parcellations

Put the stuff about rand index here A common criterion for measuring the similarity of two partitionings is Rand Index, defined as

Chapter 4

Local Search and Graph Growing Heuristics

We introduce several algorithms for generating brain parcellations. This is back to the previous chapter. Restate that we're using the edge weights as the distance correlation. The algorithms in this chapter are all local search heuristics; they begin with n unconnected vertices and iteratively join adjacent ones into components until some stopping criterion is met.

For each algorithm, the resulting parcellation is presented, discussed, and evaluated according to the criteria introduced in the previous chapter.

4.1 The Add-Edge Algorithm

The first and simplest algorithm starts with an empty graph of n vertices and sequentially adds edges between adjacent voxels in order of highest sample distance correlation, until the graph has some prespecified number of connected components k. We will refer to this algorithm as "Unconstrained Add-Edge".

The Unconstrained Add-Edge algorithm produces severely imbalanced parcellations. In the 100-component graph, there was one component containing over 99.9% of all the vertices in the graph.

Our attempt to address this problem was to impose a filter on each edge considered, adding the edge only if at least one of the two following conditions are met:

1. At least one of the two components bridge by the edge is of size less than

some prespecified parameter $s_{\min}$.

2. The union of the two components is of size $\leq s_{\max}$.

The restriction on adding new edges was not successful in creating balanced partitions.

4.1.1 Implementation of Unconstrained Version

A naive implementation of Unconstrained Add-Edge would re-compute the number of connected components in the graph (using linear-time bread-first or depth-first search) after each addition of an edge, resulting in a costly $O(EN)$ time complexity. A more efficient implementation takes advantage of the fact that each addition of an edge decreases the number of components in the graph by at most 1. Hence the algorithm needs only to compute the number of connected components after adding $c - k$ edges, where c is the current number of connected components of the graph, beginning at n.

Another implementation uses a binary search-type strategy and is $O((n+E)\log E)$. This exploits the monotonicity of our procedure which considers the ordering of the edge weights. The idea is to "search" for the last edge to add to the graph by maintaining a range of possible last edges. This isn't very clear to be honest. I would just talk about how the components must strictly grow as more edges are added, and you are just trying different number of edges to add in their sorted order. In each iteration, the algorithm would add to the graph edges 1 to the midpoint of this range, compute the number of connected components, and adjust the range based on whether the number of components is higher or lower than the target K.

4.1.2 Implementation of Size-Constrained Version using Union-Find

I think you said you'll remove this section The naive implementation must use BFS/DFS in each iteration to compute the sizes of the two components to be connected by an edge, and hence must have time complexity $O(EN)$. Fortunately, there is a way to sublinearly update information on the components of the graph, using the union-find data structure.

The core Union-Find data structure begins with an empty graph of N vertices and supports two operations. union(i, j) adds an edge between vertices i and j. root(i) returns an identifier for the component to which vertex

i belongs. All vertices in the same component have the same root. We modified Union-Find to support an additional operation. component_size(i) returns the number of vertices belonging to the component containing i.

Union-Find represents each component as a rooted tree, with vertices in the graph mapping to nodes in the tree. Information about the tree is stored in two arrays of length N, parent and size, which are subject to the following invariants.

1. For each node i, parent[i] = node i's parent on the tree, unless i is a root node. If i is a root node, then parent[i] = i.

2. Nodes i and j are in the same component if and only if they are in the same tree, if and only if they share the same root node.

3. If i is a root node, then size[i] = the size of the component, or the number of nodes in the tree. If i is not a root node, then size[i] can be anything.

A baseline implementation of the three functions is

Algorithm 1 Union-Find

```
function ROOT(i)
    while parent[i] ≠ i do
        i ← parent[i]
    end while
    return i
end function

function UNION(i, j)
    parent[root(j)] ← root(i)
end function

function COMPONENT_SIZE(i)
    return size[root(i)]
end function
```

In addition to the baseline code above, there are two important optimizations:

1. Weighted union maintains information of the sizes of each component so that the root of the smaller component always becomes a child of the larger component's root.

2. Path compression flattens the tree with each call to root. Specifically, when root is called on node i, each node traversed from i to the root has its parent set to be the root.

With these two optimizations, the time complexity of root, union, and component_size has been shown to be at least as good as $O(\log^* N)$ where $\log^*$ is the iterated logarithm, defined as the number of times the natural log must be applied to N so that it becomes less than or equal to 1.

4.2 The Edge-Contraction Algorithm and Contractible Graphs

We propose a new data structure called the *Contractible Graph* (CG) for brain parcellation. The rationale behind the CG is a heuristic procedure for partitioning a graph into somewhat balanced components so as to maximize the Adjacent-Score (Equation 3.1.2).

The CG is a mapping of the vertices of the original graph to the vertices of a new graph. The vertices of the CG are called *components* and between any two components there exists exactly one weighted edge, henceforth called a *link*. The weight of a link $w_{A,B}$ between two components A and B in the CG equals the average weight of all edges in the original graph between vertices mapped to A and vertices mapped to B. If no such edges exist, the weight of the link is 0. Formally,

$$E_{A,B} = \{(i,j) \in E : i \in A, j \in B\}$$

$$w_{A,B} = \begin{cases} \frac{1}{|E_{A,B}|} \sum_{(i,j) \in E_{A,B}} w_{ij} & \text{if } |E_{A,B}| > 0 \\ 0 & \text{otherwise} \end{cases}$$

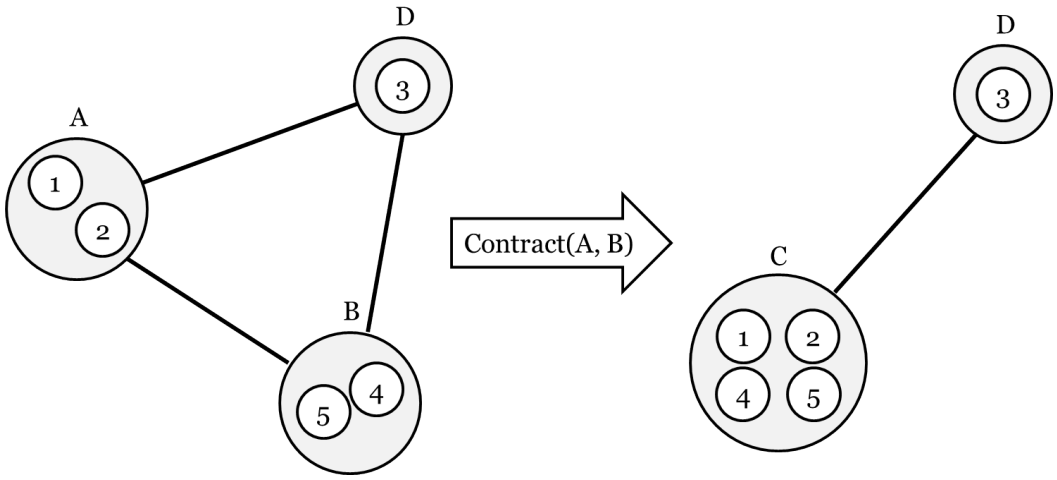

We say an edge (i, j) is *between* components A and B if i is in one of A or B and j is in the other. The *size* of a component is the number of vertices it contains. A *contraction* of a link (A, B) in a CG replaces components A and B with a new component (call it C) containing all vertices mapped to A or B, as illustrated in the figure above. Component C has one link to every other component in the CG, whose weights are the mean of the weights of the corresponding vertex edges, or 0 if no edge exists. Thus the contraction operation maintains the link-invariant property of CG. This leads to the Edge-Contraction algorithm, which begins with the original graph with all vertices as singleton components and contracts edges in a certain order until the graph has only k components in all.

Algorithm 2 Edge-Contraction

Input: Undirected positive-weighted graph G and target component number k
Create a CG from G so that every vertex maps to a unique component
repeat
  $\mathcal{S} \leftarrow$ smallest component(s) in the CG
  $(A, B) \leftarrow \underset{A \in \mathcal{S}}{\text{argmax}}\, w(A, B)$
  Contract (A, B)
until CG has k components
Output: Components of CG

Why does Edge-Contraction work better than the previous algorithms?

The Edge-Contraction algorithm attempts to address two problems of the Size-Constrained Add-Edge algorithm: unbalanced parcels and poor Adjacent-Score relative to randomized graph. It solves the former problem by prioritizing edges that are connected to small components.

The low Adjacent-Score is likely due to the following scenario: when a vertex is added to a component, it might have multiple edges to that component. One edge might have a very high weight; this is the one that is officially "added". However, the other edges with far lower weights are implicitly added as well, lowering the average edge weights within the component.

The Edge-Contraction algorithm handles this issue by maintaining that there can be at most one edge between any two components A and B, and further that the weight on such an edge is the mean of the weights on all edges that connect a vertex in A with a vertex in B.

4.2.1 Implementation using Nested Hash Tables and Priority Queue

In a Contractible Graph, the weight of the link between two components depends on the summed weight of all edges between them, and the number of such edges.

Our implementation of the CG uses *nested hash tables*, diagrammed below. The outer hash table maps each component A to an inner hash table, which maps all components B with a positive link to A to 1) the summed weights of the edges and 2) the number of edges between A and B.

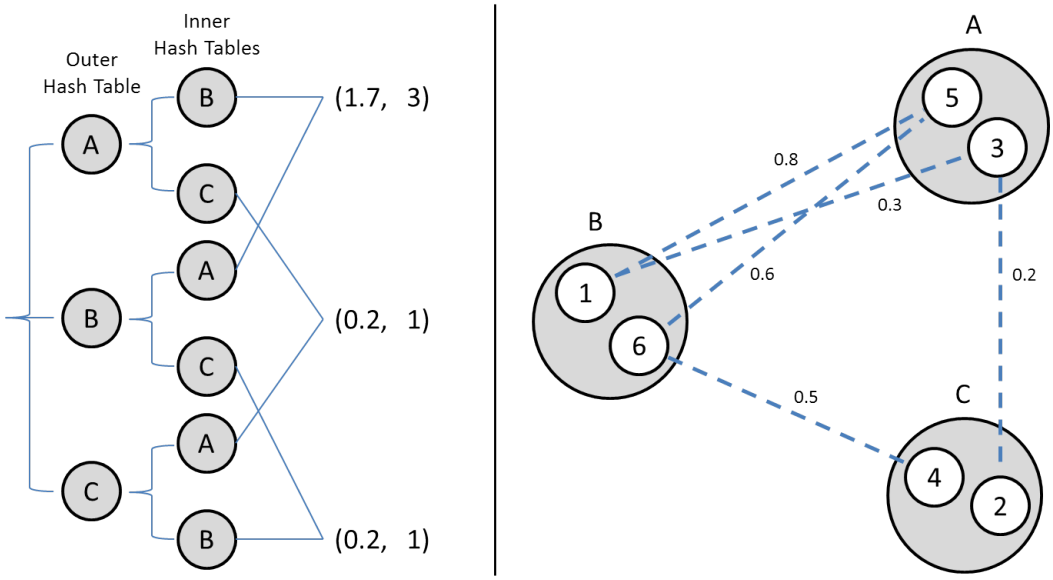

Implementing the contraction of components B and C into a new component D on this nested hash table requires the following steps. The time complexity is stated assuming no hash collisions.

1. Compute $\mathcal{X}$, the set of all components that either B or C is linked to. $O(|E_B| + |E_C|)$
2. Create a new element in the outer hash table, D, and associate it with an empty inner hash table. $O(1)$
3. For each component $X \in \mathcal{X}$,
   - Retrieve $W(X, B) + W(X, C)$, the summed weights all edges between X and B and between X and C, and $|E_{X,B}| + |E_{X,C}|$, the number of such edges. These quantities are stored explicitly as a values in the inner hash table, so this operations is $O(1)$.
   - Add a new component name D to the inner hash table of X and map it to $\big(W(X, B)+W(X, C), |E_{X,B}|+|E_{X,C}|\big)$. Delete elements B and C from the inner list of X. $O(1)$
   - In the D inner hash table, add component name X and map it to to the same $\big(W(X, B) + W(X, C), |E_{X,B}| + |E_{X,C}|\big)$. $O(1)$
4. Delete B and C from the outer list.

Having described the contraction step, we will next discuss how to efficiently locate the link to be contracted. In computer science, a *Maximum Priority Queue* (MaxPQ) data type is a set of well-ordered objects that supports the following operations:

- *add(obj)*: Adds an object to the set.
- *remove_maximum()*: Removes and returns an object with the largest priority in the set.

Using the heap data structure, the above two operations both run in $O(\log n)$ time.

Each component on the CG will be associated with an element of the priority queue. The priority of component A is defined as

$$\max_X \ w_{A,X} - |A|$$

Since our graph link and edge weights are all between 0 and 1, the highest priority element in the queue always has the smallest size. Therefore, if the priority queue is up-to-date with the CG, the next link to be contracted according to Edge-Contraction has an endpoint component whose priority is the highest in the queue.

However, a complication arises from the fact that a contraction can change the priorities of components neighboring the contracting components, thereby making the priorities stored in the MaxPQ out-of-date. For instance, if components A and B are contracted, and there is a component C with positive links to both A and B, then the $C-A$ and $C-B$ links will be replaced by a $C-(AB)$ link with a different weight. If either $C-A$ or $C-B$ links happened to be the maximum-weighted links of C, then C's priority will be lower, and C ought to be further down the queue.

To address this issue, we could re-compute the priority of every component drawn from the MaxPQ. If the component's actual priority is not the maximum, then it is re-inserted into the queue with updated priority. Additionally, the maximum priority component may no longer exist in the CG due to contraction with another component. In this case it is simply discarded.

Without using an efficient priority queue, the linear searching method of finding the next link to contract results in a $O\big(n(n-k)\big)$ time algorithm. Using the priority queue the time complexity of Edge-Contraction is $O\big((n-k)(m+\log n)\big)$, where m is the average number of positive links a component has.

Table 4.1: Results of Edge-Contract for Different Component Numbers

Number of Components	Adjacency	Multi-Boundary	Jaggedness	Balance
500	0.7991	0.7578	54.65	0.327
400	0.7990	0.7723	59.20	0.343
300	0.7974	0.7921	65.20	0.297
250	0.7955	0.7991	69.51	0.356
200	0.7941	0.8101	75.47	0.357
150	0.7931	0.8225	83.88	0.418
116	0.7913	0.8389	92.14	0.439
100	0.7911	0.8488	97.63	0.383
AAL	0.7225	——	29.62	0.332

4.2.2 Results

The Edge-Contract parcellations notably outperformed the anatomical AAL parcellation in the Adjacency-Score. For further comparison, found the mean edge weight in the graph to be 0.7258, which is even slightly higher than the average adjacent within-parcel edge in AAL. This suggests that the AAL parcellation has no connection with the functional information contained in this fMRI data set. It shows on the other hand that the Edge-Contract algorithm can successfully locate regions of functional similarity.

The one apparent deficiency of Edge-Contract is the jaggedness of its parcels. Comparison of our parcellations with the AAL shows that our 116-component parcellation – the same number of components as AAL – has an average parcel surface area roughly $\left(\frac{92.14}{29.62}\right)^{\frac{2}{3}} \approx 2.11$ times that of AAL. Visually, that difference is shown in the plots below of a typical component from each parcellation. Include a citation to the plots (where are they :o?)

4.3 The Generalized Edge-Contraction Algorithm

In the original Edge-Contraction algorithm, the criteria for selecting the next link to contract was to search through the set of smallest components and find the link of maximal weight. Because this criteria takes no account of the shape of the two components to be contracted, the resulting parcels tend to be very jagged.

Table 4.2: Results of Generalized Edge-Contract for Various Parameter Settings

α	β	Adjacent	Jaggedness	Balance
3	1	0.7500	25.3	0.285
6	1	0.7574	31.0	0.231
10	1	0.7634	36.6	0.211
6	2	0.7565	31.0	0.199
6	4	0.7576	30.9	0.270

(a) 116 Parcels

α	β	Adjacent	Jaggedness	Balance
3	1	0.7592	23.8	0.218
6	1	0.7651	28.0	0.143
10	1	0.7705	32.0	0.221
6	2	0.7670	28.2	0.169
6	4	0.7669	28.8	0.293

(b) 300 Parcels

To address this we expanded the criterion for finding the next link to contract. Rather than use only the size of the component and the weight of the link, a *Generalized Edge-Contraction* algorithm may use any piece of information stored in the Contractible Graph about a pair of components, such as the number of edges connecting two components. A *priority function* takes information of any two components in a CG and outputs a real number, the priority. For each iteration, the pair of components with the largest priority is contracted and the priorities of neighboring components with respect to the newly conjoined component are computed.

For two components A, B let $|A|$ denote size (number of vertices) of A, $E_{A,B}$ denote the set of edges between A and B, and $w_{A,B}$ the weight of the link connecting A and B. The priority function of the original Edge-Contraction algorithm is $p_0(A, B) = w_{A,B} - |B|$.

Be sure the include a in-text citation to these tables

A link (A, B) will have high priority if either component is small, if the link has a large weight, and if it has a good boundary-ratio, defined as $\frac{|E_{A,B}|}{\min(|A|,|B|)}$, which helps to minimize jaggedness. From these notions we created a family of priority functions indexed by tunable parameters α and

β

$$p_1(A, B) = \frac{w_{A,B}^{\alpha}}{|A|^{\beta}} \cdot \frac{|E_{A,B}|}{\min(|A|, |B|)} \tag{4.1}$$

that modulate the balance of small size, large weight, and high boundary ratio. Table 4.2 shows the results of the 116-component and 300-component Generalized Edge-Contract parcellation when performed for various values of α and β. The adjacent scores have fallen on average from 0.79 in the vanilla edge contraact to 0.75 here. This implies a tradeoff between prioritizing edge weight, jaggedness, and balance in producing a parcellation.

With a balance score of 0.332, the AAL parcellation was better balanced than all of the parcellations obtained via this priority function, though not drastically. In terms of jaggedness, these parcellations all fell within the vicinity of AAL. In this one brain, the best parcellation arises from parameters $\alpha = 6$ and $\beta = 4$.

Parcellations of other brains using generalized edge contract can be found in chapter 8.

Chapter 5

Spectral Methods

In the previous chapter, we showed how local search heuristics produced parcels that were balanced and had high within-parcel and low between-parcel edge weights. The central idea behind such methods was to choose vertices to be in the same component if the edge connecting them has high distance correlation. Vertices were added to components one-by-one with constraints on component size, but not on component shape. As a result, one salient issue with these parcellations was the lack of smoothness in the boundaries between parcels There was scant resemblance between the anatomical maps of the brain depicting smooth, rotund lobes and our jagged, web-like parcellations.

One key reason for this phenomenon are the local search heuristics' focus on maximizing *average* within-component edge weights (equivalently, minimizing *average* between-component edge weights). To get smoothness in the boundary between components, we could either impose a penalty for too many between-component edges and work that into the local search heuristics, or try minimizing over the sum of all weights on between-component edges. This chapter deals with the second approach and this family of methods is called spectral partitioning.

Spectral partitioning constitutes the second major class of techniques used to partition graphs. Rather than rely on local component-growing heuristics, spectral partitioning uses information about the entire graph at once.

Throughout this chapter, a valid partitioning $P_k = (V_1, ..., V_k)$ of the graph $G = (V, E)$ is defined in the same way as in Chapter 3; i.e., it must satisfy

1. $V_i \neq \varnothing$ for all $V_i \in \mathcal{P}_k$
2. $\bigcup_{i=1}^{k} V_i = V$
3. $V_i \cap V_j = \varnothing$ for all $V_i, V_j \in \mathcal{P}_k$
4. V_i is connected (i.e. for every two vertices in V_i, there is a path between them) for all $V_i \in \mathcal{P}_k$.

For all edges $(i, j) \in E$, let w_{ij} denote the weight of the edge connecting vertices i and j. $S^{n\times n}$ is the set of real symmetric $n \times n$ matrices. We further define, for a given graph $G = (V, E)$, the associated adjacency matrices and degree matrices, defined below.

Definition 5.0.1 (Adjacency matrix) *Let G be a graph with weights ω. The corresponding adjacency matrix $A \in \mathcal{S}^{n\times n}$ has entries*

$$A_{ij} = \begin{cases} w_{ij} & \text{if } (i,j) \in E \\ 0 & \text{otherwise.} \end{cases}$$

Definition 5.0.2 (Degree matrix) *Let G be a graph with weights ω, and A be the corresponding adjacency matrix. The corresponding degree matrix $D \in \mathcal{S}^{n\times n}$ is formed by*

$$D_{ij} = \begin{cases} \sum_{k=1}^{n} A_{ik} & \text{if } i = j \\ 0 & \text{otherwise.} \end{cases}$$

5.1 Size-Constrained MinCut and Graph Bipartitioning

Consider the case of partitioning a graph into two components, $k = 2$. For all vertices $i \in V$, let $x_i = 1$ if $i \in V_1$ and $x_1 = -1$ if $i \in V_2$. Then the sum of weights on edges between the two components is

$$\begin{aligned} C(P_2) &= \sum_{i\in V_1} \sum_{j\in V_2} A_{ij} \\ &= \sum_{i=2}^{n} \sum_{j=1}^{i-1} \frac{(x_i - x_j)^2}{4} A_{ij} \end{aligned}$$

since

$$(x_i - x_j)^2 = \begin{cases} 4 & \text{if } i,j \text{ are in different components} \\ 0 & \text{otherwise.} \end{cases}$$

$C(P_2)$ can also be written in a matrix quadratic form, as

$$\begin{aligned}
C(P_2) &= \sum_{i=2}^{n} \sum_{j=1}^{i-1} \frac{(x_i - x_j)^2}{4} A_{ij} \\
&= \frac{1}{2} \sum_{i,j=1}^{n} \frac{(x_i - x_j)^2}{4} A_{ij} \\
&= \frac{1}{2} \sum_{i,j=1}^{n} \frac{x_i^2 + x_j^2 - 2x_i x_j}{4} A_{ij} \\
&= \frac{1}{2} \sum_{i,j=1}^{n} \frac{1 - x_i x_j}{2} A_{ij} \\
&= \frac{1}{4} \sum_{i,j=1}^{n} (x_i^2 - x_i x_j) A_{ij} \\
&= \frac{1}{4} \sum_{i=1}^{n} x_i^2 \sum_{j=1}^{n} A_{ij} - \frac{1}{4} \sum_{i,j=1}^{n} x_i A_{ij} x_j \\
&= \frac{1}{4} \sum_{i=1}^{n} x_i^2 D_{ii} - \frac{1}{4} x^T A x \\
&= \frac{1}{4} x^T (D - A) x \\
&= \frac{1}{4} x^T L x,
\end{aligned}$$

where L is called the Laplacian matrix of the graph and defined as $L = D - A$. MinCut can thus be formulated as minimizing $x^T L x$ subject to $x \in \{-1, 1\}^n$.

Algorithms like Karger's can solve MinCut in polynomial time. However, MinCut in this formulation lacks constraints on the size of the partitions, and if applied to our brain parcellation problem, would result in severely inbalanced partitions. If constraints on the sizes of the components were added, the problem becomes NP-hard in the general case [Buluç et al., 2013].

An old but effective approach to bipartitioning uses the eigenvectors of the Laplacian matrix and is called spectral bipartitioning. The approach relaxes the $\{-1, 1\}$ constraint on x (and rescales x) so that it need only satisfy $\|x\| = 1$ ($\|\cdot\|$ here refering to L2 norm). It is easy to see that $\left\{x : x \in \{-\frac{1}{\sqrt{n}}, \frac{1}{\sqrt{n}}\}^n\right\} \subset \left\{x \in \mathbb{R}^n : \|x\| = 1\right\}$. The problem now becomes

$$\begin{aligned} \min_{x} \quad & x^T L x \\ \text{s.t.} \quad & \|x\| = 1. \end{aligned} \tag{5.1}$$

Using Lagrangian multipliers, it can be shown that all optimal solutions to the above must satisfy $Lx = \lambda x$ and this problem reduces to finding the smallest eigenvalues of L and their associated eigenvectors. In addition, 5.1.1 below implies that all eigenvalues are nonnegative.

Theorem 5.1.1 *Let L be a Laplacian matrix. Then $L \succeq 0$ (L is positive semidefinite)*

Proof. *Let $x \in \mathbb{R}^n$. $x^T L x = x^T D x -$ Can omit proof*

Note that from the $C(P_2) = \sum_{i>j} \frac{(x_i - x_j)^2}{4} A_{ij} = \frac{1}{4} x^T L x$ equivalence we know that 0 and $(\frac{1}{\sqrt{n}}, ..., \frac{1}{\sqrt{n}})^T$ is a minimum eigenvalue and eigenvector to this system. For bipartitioning, the useful eigenvector is the one that corresponds to the 2nd smallest eigenvalue, which is nonzero if the graph as a whole is connected. We'll denote this eigenvalue as λ_1 and corresponding unit eigenvector as x_1. We have the following:

Theorem 5.1.2 *Let P_2 be any valid partition into 2 components. Then $C(P_2) \geq \lambda_1$*

Proof. *Can omit proof*

In the literature, x_1 is often referred to as the Fiedler vector, after the first mathematician who studied it in detail. From the Fiedler vector we can obtain a variety of "good" bipartitions. We can impose a size constraint $|V_1| = s$ and obtain a bipartition satisfying this by placing the vertices associated with the s largest entries of x_1 in V_1. This encompasses bipartitions of equal component size. We can also sort the entries of x_1 and find the largest difference between consecutive sorted entries. Vertices corresponding to entries sorted to the left of this split can be placed in V_1 and vertices sorted to the right in V_2. This method tends to approximate the MinCut solution.

The result of spectral bipartitioning on a resting state fMRI scan is shown below. As anticipated, the boundaries of between the components are smooth. Cite the figure numbers intext since Latex might put the figures far away from the text.

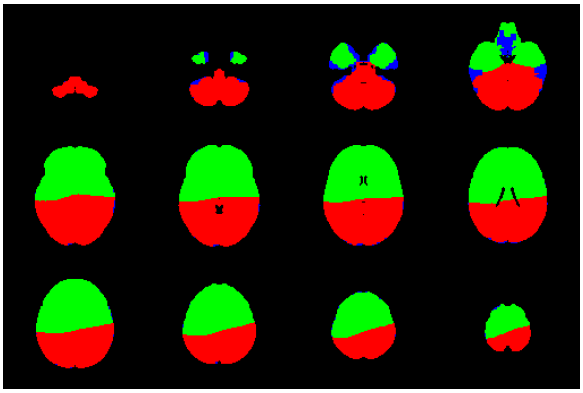

Axial

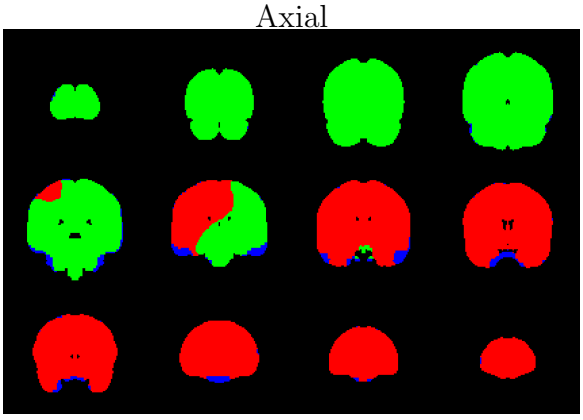

Coronal

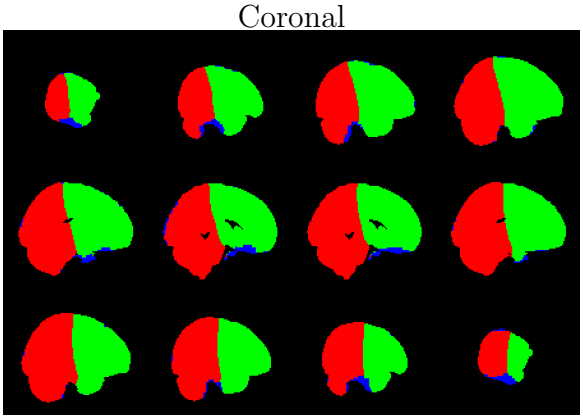

Sagittal

One can recursively apply this bipartitioning method to the component subgraphs to obtain k-partitions, but there is a more elegant approach involving additional eigenvectors that requires the construction of only one Laplacian matrix, which we shall discuss next.

5.2 Spectral k-partitioning

We'll begin with two definitions to set up the machinery for partitioning into k components.

Definition 5.2.1 (Assignment matrix) *$X \in \{0,1\}^{n \times k}$ has entries*

$$X_{ih} = \begin{cases} 1 & \text{if vertex } i \in V_h \\ 0 & \text{otherwise.} \end{cases}$$

Let u_m denote a vector of m ones. An assignment matrix characterizes a valid partition only if it satisfies $Xu_k = u_n$ and $X^T u_n > 0$. The columns of X are orthogonal.

Definition 5.2.2 *[Partition matrix] $P \in \{0,1\}^{n \times n}$ has entries*

$$P_{ij} = \begin{cases} 1 & \text{if vertices } i \text{ and } j \text{ are in the same component} \\ 0 & \text{otherwise.} \end{cases}$$

If P and X refer to the same partitioning, then $P = XX^T$.

In the k-component case, we define the weight of a partition $C(P_k)$ as the sum of weights of edges between different components (between-edges). This is equivalent to the definition below:

Definition 5.2.3 (Cut weight) *For a partition $P_k = (V_1, ..., V_k)$, the cut weight is defined as*

$$C(P_k) = \sum_{h=1}^{k} E_h$$

where E_h is the sum of the weights of all edges with one vertex in V_h and one vertex not in it.

This is equal to the sum of the weights of all edges in the graph minus the sum of the weights of all edges connecting vertices in the same component (within-edges).

In addition, if D is the degree matrix, then

$$\begin{aligned}\mathrm{Tr}(PD) &= \sum_{i,j=1}^{n} P_{ij}D_{ij} \\ &= \sum_{i=1}^{n} P_{ii}D_{ii} \\ &= \sum_{i=1}^{n} P_{ii}\sum_{j=1}^{n} A_{ij} \\ &= \sum_{i=1}^{n}\sum_{j=1}^{n} A_{ij}\end{aligned}$$

is the sum of the weights of all edges in the graph. Similarly, $\mathrm{Tr}(PA)$ equals the sum of weights of all within-edges. It follows that

$$C(P_k) = \mathrm{Tr}(X^T L X).$$

The problem of minimizing this quadratic function subject to the constraint that X must be a valid assignment matrix is called (minimum) k-cut and is NP-complete for arbitrary k [Goldschmidt and Hochbaum, 1994].

Even if a polynomial time algorithm existed for minimizing $C(P_k)$, there would be no guarantee that the resulting partitions would be balanced. To address this issue, researchers have developed a similar cost objective called the *ratio-cut cost*.

Definition 5.2.4 (Ratio-cut cost) *For a given partition $P_k = (V_1, ..., V_k)$ the ratio-cut cost C_R is defined*

$$C_R(P_k) = \sum_{h=1}^{k} \frac{E_h}{|V_h|}$$

where E_h is the sum of the weights of all edges with one vertex in V_h and one vertex not in it.

The ratio-cut cost places an implicit penalty on small components and therefore encourages balanced component sizes. Associated with ratio-cut objective there is a new decision variable called the *ratioed assignment matrix*.

Definition 5.2.5 (Ratioed Assignment Matrix) *$R \in \mathbb{R}^{n \times k}$ has entries*

$$R_{ih} = \begin{cases} \frac{1}{\sqrt{|V_h|}} & \text{if vertex } i \in V_h \\ 0 & \text{otherwise} \end{cases}$$

We note that R has the same form as the assignment matrix X except with columns rescaled so that the column sum is $\sqrt{|V_h|}$ for each component V_h. Similarly there is also a *ratioed partition matrix* equal to RR^T, with entries $[RR^T]_{ij} = \frac{1}{|V_h|}$ if $i, j \in V_h$ and 0 otherwise.

The ratioed assignment matrix relates to the ratio-cut cost in the same way the assignment matrix relates to cut weight; namely, if R characterizes a partition P_k then

$$C_R(P_k) = \mathrm{Tr}(R^T L R).$$

Here, R has the additional useful property that $R^T R = I$.

In fact, for any matrix R satisfying

1. $R^T R = I$
2. $R \geq 0$ (element-wise)
3. $RR^T u_n = u_n$ where u_n is a n-dimensional vector of all ones.

there is a valid partition whose ratioed assignment matrix equals R. The third constraint ensures that all non-zero entries of R equal $\frac{1}{\sqrt{|V_h|}}$.

Minimizing $C_R(P_k)$ over the set of valid R matrices is an NP-hard combinatorial optimization problem (?) Citation needed. The spectral relaxation first proposed in [Chan et al., 1994] drops the second and third constraints on R and the resulting problem (shown below) has a closed-form optimal solution.

$$\begin{aligned} \min_{R \in \mathbb{R}^{n \times k}} \quad & \mathrm{Tr}(R^T L R) \\ \text{s.t.} \quad & R^T R = I \end{aligned} \tag{5.2}$$

[Fan, 1950] proved that an optimal solution $\hat{R}$ to the above has columns equaling k orthonormal eigenvectors corresponding to the k smallest eigenvalues of L: λ_1, λ_2, ..., λ_k. Furthermore, the optimal objective value, $\mathrm{Tr}(\hat{R}^T L \hat{R}) = \sum_{h=1}^{k} \lambda_h$. Analogously to $P = XX^T$, $\hat{R}$ can be thought of as n k-dimensional points where the dot products of the ith and jth rows measure the affinity of vertices i and j to be in the same component.

As [Chan et al., 1994] pointed out, recovery of the discrete assignment matrix X from the continuous assignment matrix $\hat{R}$ would be more accurate if $\hat{R}$ were un-ratioed (i.e. if each row of R had the same length), since the ratioed assignment matrix R has the problematic property that for any i, j in the same component, the dot product $R_i^T R_j$ depends on the size of that component. The un-ratioed version of $\hat{R}$ be recovered by dividing each row by its Euclidean norm. The result, $\hat{X}$, can be thought of as n points in $\mathbb{R}^k$ embedded on the surface of the unit hypersphere.

Obtaining the partition assignment matrix X, from this spherical embedding is a clustering problem. We used k-means with cosine similarity $s(x, y) = x^T y$ for this purpose. For each cluster h and its associated points matrix $H \in \mathbb{R}^{m \times k}$, the location of the cluster centroid c_h in the next iteration satisfies $\sum_{i=1}^{m} H_i = \lambda c_h$ for some positive scalar λ such that $\|c_h\| = 1$.

To summarize, [Chan et al., 1994] introduced a spectral relaxation of the graph k-partitioning to minimize the ratio cut. From the Laplacian matrix's smallest k eigenvectors we obtain a continuous approximation $\hat{R}$ to the optimal ratioed assignment matrix R. The rows of $\hat{R}$ are standardized to length 1 to get the continuous approximation $\hat{X}$ to optimal (unratioed) assignment matrix X. Following standard practice we used k-means clustering with cosine similarity to recover the component assignments from $\hat{X}$.

Chapter 6

Symmetric Nonnegative Matrix Factorization

In the previous chapter, we showed that the problem of finding the minimum ratio cut of a graph (with Laplacian matrix L, degree matrix D, and adjacency matrix A) can be formulated as minimizing

$$\mathrm{Tr}(R^T L R) \tag{6.1}$$

over the set, $\mathcal{R}$, of $n \times k$ matrices satisfying

1. $R^T R = I$
2. $R \geq 0$ (element-wise)
3. $RR^T u_n = u_n$ where u_n is a n-dimensional vector of all ones.

If the sizes of the components in the optimal ratio cut partition are perfectly balanced, which is equivalent to saying if the diagonal of the optimal ratioed assignment matrix RR^T has entries all equal to k/n, then

$$\begin{aligned}
\mathrm{Tr}(R^T D R) &= \sum_{i=1}^{n} [RR^T]_{ii} D_{ii} \\
&= \sum_{i=1}^{n} \frac{k}{n} D_{ii} \\
&= \frac{k}{n} \sum_{i,j} A_{ij}
\end{aligned}$$

is a constant that does not depend on R. The same is true if each vertex has the same degree $D_{ii} = d$, in which case

$$\begin{aligned}\mathrm{Tr}(R^T DR) &= \sum_{i=1}^{n} [RR^T]_{ii} D_{ii} \\ &= d \sum_{i=1}^{n} [RR^T]_{ii} \\ &= dk\end{aligned}$$

is also a constant that does not depend on R. In either case,

$$\underset{R \in \mathcal{R}}{\operatorname{argmin}} \ \mathrm{Tr}(R^T LR) = \underset{R \in \mathcal{R}}{\operatorname{argmax}} \ \mathrm{Tr}(R^T AR).$$

This equality may also hold even if neither condition is true, especially if they are approximately true.

Spectral k-partitioning drops the second and third constraints of $\mathcal{R}$ to derive a closed-form minimizer of 6.1, from which the original assignment matrix can be obtained by k-means. This chapter deals with an alternative relaxation of $\mathcal{R}$ that drops the first and third constraints.

6.1 Symmetric Nonnegative Matrix Factorization

For an $n \times m$ matrix A, a nonnegative matrix factorization (NMF) is a pair of matrices $W \in \mathbb{R}^{n \times k}$ and $H \in \mathbb{R}^{m \times k}$ that minimizes $\|A - WH^T\|_F^2$ subject to elementwise nonnegativity: $H \geq 0$ and $W \geq 0$. Here, $\|X\|_F = \sqrt{\sum_{ij} X_{ij}}$ refers to the Frobenius norm.

For $n \times n$ symmetric matrices A, a *symmetric* NMF (SymNMF) is a matrix $H \in \mathbb{R}^{n \times k}$ that minimizes $\|A - HH^T\|_F^2$, and k is an arbitrary positive integer typically much smaller than n.

The following theorem from [Ding et al., 2005] illustrates the connection between SymNMF and graph partitioning.

Theorem 6.1.1 *Let A be a $n \times n$ symmetric matrix. Then*

$$\underset{H^T H = I, H \geq 0}{\operatorname{argmax}} \ \mathrm{Tr}(H^T AH) = \underset{H^T H = I, H \geq 0}{\operatorname{argmin}} \ \|A - HH^T\|_F^2.$$

Proof.

$$\begin{aligned}\underset{H^TH=I,H\geq 0}{\operatorname{argmax}} \operatorname{Tr}(H^TAH) &= \underset{H^TH=I,H\geq 0}{\operatorname{argmin}} -2\operatorname{Tr}(H^TAH) \\ &= \underset{H^TH=I,H\geq 0}{\operatorname{argmin}} \operatorname{Tr}(AA^T) - 2\operatorname{Tr}(H^TAH) + \|H^TH\|_F^2 \\ &= \underset{H^TH=I,H\geq 0}{\operatorname{argmin}} \|A - HH^T\|_F^2.\end{aligned}$$

If A is the adjacency matrix, then under the equal vertex degrees condition described earlier $\underset{H^TH=I,H\geq 0}{\operatorname{argmax}} \operatorname{Tr}(H^TAH) = \underset{H^TH=I,H\geq 0}{\operatorname{argmin}} \operatorname{Tr}(H^TLH)$. Hence an alternative approach to the minimum ratio-cut problem is to drop the $H^TH = I$ constraint and solve the SymNMF problem:

$$\begin{aligned}\min_{H\in\mathbb{R}^{n\times k}} \quad & \|A - HH^T\|_F^2 \\ \text{s.t.} \quad & H \geq 0.\end{aligned} \tag{6.2}$$

This relaxation has two key differences from the spectral relaxation:

1. There is no closed-form solution, and the optimal value is found via an optimization algorithm, described in the next section.

2. The optimal assignments are recovered directly from the largest entry in each row. There is no need for k-means.

6.1.1 The Alternating Nonnegative Least Squares Algorithm

The algorithm for solving (6.2) developed by [Kuang et al., 2015] uses the same framework as existing algorithms for solving the asymmetric NMF problem: $\min_{W,H\geq 0} \|A - WH^T\|_F^2$. That framework, called *alternating nonnegative least squares* is an iterative scheme that fixes one of the matrix factors and solves for the other. Then, it fixes the factor just solved and solves for the first. In other words, these two steps are repeated until convergence:

1. $W \leftarrow \underset{W\geq 0}{\operatorname{argmin}} \|A - WH^T\|_F^2$

2. $H \leftarrow \underset{H\geq 0}{\operatorname{argmin}} \|A - WH^T\|_F^2$

One reason this method is effective in the asymmetric case is that the two subproblems are convex, so it is easy to attain the global minimum in each subproblem. Further, a number of specialized algorithms have been developed to solve these nonnegative least squares problems quickly. One in particular by [Kim and Park, 2011] works well with large, sparse A matrices and is detailed in the next subsection.

An approach for SymNMF in [Kuang et al., 2015] uses this framework by artificially creating two different factors rather than one and adding on an adjustable penalty term for the difference between the two factors:

$$\min_{W,H\geq 0} \|A - WH^T\|_F^2 + \alpha\|W - H\|_F^2 \tag{6.3}$$

where $W, H \in \mathbb{R}^{n\times k}$. As in the asymmetric case, the algorithm computes W and H iteratively by fixing one of the two factors. The difference is the introduction of the penalty term, α, which can be increased after each iteration to force the eventual convergence of W and H.

(6.3) can also be re-written in the same form as the asymmetric NMF:

$$\left\| \begin{bmatrix} W \\ \sqrt{\alpha} I_k \end{bmatrix} H^T - \begin{bmatrix} A \\ \sqrt{\alpha} W^T \end{bmatrix} \right\|_F^2 \tag{6.4}$$

with $\begin{bmatrix} W \\ \sqrt{\alpha} I_k \end{bmatrix}$ taking on the part of the fixed matrix and H the decision matrix. The ANLS algorithm for SymNMF is the following:

Algorithm 3 ANLS algorithm for SymNMF

1: Initialize H
2: **repeat**
3: $\quad W \leftarrow H$
4: $\quad H \leftarrow \underset{H\geq 0}{\operatorname{argmin}} \left\| \begin{bmatrix} W \\ \sqrt{\alpha} I_k \end{bmatrix} H^T - \begin{bmatrix} A \\ \sqrt{\alpha} W^T \end{bmatrix} \right\|_F^2$
5: $\quad$ increase α
6: **until** convergence

[Kuang et al., 2015] recommends multiplying α by 1.01 each iteration. The next section describes the method in [Kim and Park, 2011] for solving the embedded nonnegative least squares problem.

6.1.2 Block Pivoting Algorithm for Nonnegative Least Squares

Let us consider a simplified form of the NLS step in Algorithm 3. Let x denote a single k-dimensional row of H, and our goal is to solve

$$\min_{x \geq 0} \|Cx - b\|_2^2 \tag{6.5}$$

where $C = \begin{bmatrix} W \\ \sqrt{\alpha} I_k \end{bmatrix}$ and b is the column of $\begin{bmatrix} A \\ \sqrt{\alpha} W^T \end{bmatrix}$ with the same index as the index of row x in H. Since the rows of H share no constraints with one another, the general NLS problem in Algorithm 3 can be viewed simply as n independent cases of Equation 6.5. In general, be sure the write the word "Equation" in front of all equation citations.

The Karush-Kuhn-Tucker necessary conditions for optimality are:

1. $y = C^T Cx - C^T b$,
2. $y \geq 0$,
3. $x \geq 0$,
4. $x_i y_i = 0$ for $i = 1, ..., k$.

Since I_k is full column rank, so is C, making $C^T C$ positive definite and Equation 6.5 strictly convex.

Let x^* be the optimal solution to Equation 6.5. Suppose the indices of the strictly positive entries of x^* were known and denote them with F. Then all the entries of x^* and y^* can be computed. Let x_F denote the vector of entries of x indexed by F and C_F is the matrix of *columns* of C indexed by F. Let G be all the elements of $\{1, ..., k\}$ not in F. Then,

$$x_F = \operatorname*{argmin}_{x_F \geq 0} \|C_F x_F - b\|_2^2, \tag{6.6a}$$

$$x_G = 0, \tag{6.6b}$$

$$y_F = 0, \tag{6.6c}$$

$$y_G = C_G^T (C_F x_F - b). \tag{6.6d}$$

Equation 6.6a is implied by the fact that the strictly positive entries of x must solve the unconstrained problem. Equation 6.6b is true by definition

of F and G. (6.6c) is implied by KKT condition 4. Equation 6.6d is implied by KKT condition 1. If index sets F and G give the optimal solution, then x_F and y_G must satisfy KKT conditions 2 and 3 (nonnegativity). Therefore the *Block Pivoting Algorithm* finds the optimal x and y by searching for the correct F and G index sets.

Suppose the x and y computed from the current F and G do not satisfy the KKT conditions, or equivalently the set

$$V = \{j \in F : x_j < 0\} \cup \{j \in G : y_j < 0\} \tag{6.7}$$

is not empty. The algorithm updates F and G by taking a subset $\hat{V} \subseteq V$ and setting

$$F \leftarrow (F - \hat{V}) \cup (\hat{V} \cap G), \tag{6.8a}$$

$$G \leftarrow (G - \hat{V}) \cup (\hat{V} \cap F). \tag{6.8b}$$

By default, the algorithm uses $\hat{V} = V$ for speed. However, there are cases where this could result in an infinite loop, so the single pivot rule $\hat{V} = \max\{j \in V\}$ is invoked instead, despite being slower.

In the multicolumn case, we solve

$$\min_{X \geq 0} \|CX - B\|_2^2 \tag{6.9}$$

where X is $k \times n$ matrix, and the algorithm needs to track, for each column of X, the F and G indices. Since in many cases including ours, $n \gg k$, so many columns of X are likely to have the same F and G. Given this fact, the block pivoting algorithm has a shortcut to solving Equation 6.6a and Equation 6.6d for each column. Equation 6.6a is found by solving $C_F^T C_F x_F = C_F^T b$ and the Cholesky factorization for this can be done just once for all columns with the same F indices. Additionally, the $C_F^T C_F$, $C_F^T b$, $C_G^T C_F$, and $C_G^T b$ matrices and vectors required to compute x_F and y_G can be extracted as submatrices of $C^T C$ and $C^T B$, computed once in the beginning of the algorithm. In our SymNMF case, these two matrices are much smaller than the original sparse A matrix that formed them.

$$C^T C = W^T W + \alpha I_k \tag{6.10}$$

$$C^T B = W^T A + \alpha W^T \tag{6.11}$$

You mentioned this isn't done yet.

Algorithm 4 Block Pivoting Algorithm for NLS

Input: $A \in \mathbb{R}^{n\times n}$, $W \in \mathbb{R}^{n\times k}$
Output: X
Compute C^TC and C^TB by (6.10) and (6.11)
Initialize $F_i = \varnothing$ and $G_i = \{1, ..., k\}$ for all $i = 1, ..., n$
Initialize $\alpha(\in \mathbb{R}^n) = 3$ and $\beta(\in \mathbb{R}^n) = k + 1$
repeat
  Update X and Y according to F and G by column-grouping.
  $I \leftarrow \{i : (X_{F_j}, Y_{G_j}) \text{ is infeasible}\}$
  for all $i \in I$ **do**
    Compute V_i by (6.7)
    if $|V_i| < \beta_i$ **then**
      $\beta_i \leftarrow |V_i|$
      $\alpha_i \leftarrow 3$
      $\hat{V}_i \leftarrow V_i$
    else if $\alpha_i \geq 1$ **then**
      $\alpha_i \leftarrow \alpha_i - 1$
      $\hat{V}_i \leftarrow V_i$
    else if $\alpha_i = 0$ **then**
      $\hat{V}_i = \max\{j \in V_i\}$
    end if
    Update F_i and G_i by (6.8)
  end for
until $I = \varnothing$

6.2 Connected Partitions

An issue with the SymNMF approach is that the partitions may not be connected – there may exist a vertex, none of whose neighbor vertices belong to the same parcel that it does.

Definition 6.2.1 (Unweighted Adjacency Matrix) *For a graph with n vertices and edge set E, the unweighted adjacency matrix $B \in \{0,1\}^{n\times n}$ has entries*

$$B_{ij} = \begin{cases} 1 & \text{if } (i,j) \in E \\ 0 & \text{otherwise} \end{cases}$$

Proposition 6.2.2 *Let B be the unweighted adjacency matrix of a graph with n vertices and $X \in \{0,1\}^{n\times K}$ be an assignment matrix satisfying $Xe_K = e_n$ and $X^T e_n \geq e_K$. If the partitions of the graph defined by X are connected then*

$$(B - I)X \geq 0.$$

Proof Let b_i denote the ith row of B and X_k the kth column of X. Since the non-zero entries of b_i indicate which vertices i is neighboring and the non-zero entries of X_k indicate which vertices are in the kth partition, the dot product $b_i X_k$ equals the number of vertices neighboring i that are in the kth partition.

If the partitions of the graph are connected, then this number is at least 1 if k is the partition containing i. If k does not contain i, then $b_i X_k$ can be 0. This can be succinctly expressed as $b_i X_k \geq X_{ik}$ for all $i = 1, ..., n$ and $k = 1, ..., K$, which is equivalent to the matrix inequality above. ■

This fact will be used in the next section for the problem of finding a binary matrix factorization of A.

6.3 Symmetric 0-1 Matrix Factorization

The SymNMF method of graph partitioning finds continuous nonnegative matrix $H \in R^{n\times k}$ so as to minimize $\left\|A - HH^T\right\|_F^2$ and obtains the 0-1 assignment matrix X by thresholding H. In the graph partitioning case, it arguably more desirable to obtain binary X directly rather than via the continuous H.

This leads us to the *Symmetric Binary Matrix Factorization* problem, henceforth called SymBMF. Formally, for a symmetric matrix $A \in [0,1]^{n \times n}$ we want to solve

$$\begin{array}{ll} \text{minimize} & \left\|A - XX^T\right\|_F^2 \\ \text{subject to} & X \in \{0,1\}^{n \times k} \\ & Xe_k = e_n. \end{array}$$

The constraint $X^T e_n \geq 1$ can be added to ensure no column of X contains all zeros. Additionally, the constraint $(B-I)X \geq 0$ (where B is the unweighted adjacency matrix) can be added for graph partitioning purposes to ensure all the partitions are connected (Equation 6.2.2).

It is desirable for algorithms that solve SymBMF to work well when A is sparse or incomplete. In the sparse case, when most entries of A are zero, the complexity of the algorithm ideally ought to scale with the number of non-zero entries, and not with the number of rows and columns. Similarly in the case of incomplete A there are entries of A that are unknown or that we simply don't care about approximating. This changes the objective function from a matrix norm to a summation:

$$\sum_{(i,j) \in A} (A_{ij} - x_i^T x_j)^2$$

where x_i denotes the ith row of X.

We present two methods that both scale well in sparse A and can handle incomplete A. The first is a very fast local minimizer inspired by methods from multidimensional scaling. The second is a mixed integer program that solves the problem globally, but is not as efficient.

6.3.1 Component Switching

The central idea behind this to begin with an random $n \times k$ binary matrix X that satisfies $Xe_k = e_n$ and iteratively edit each row of X so as to minimize $\|A - XX^T\|_F^2$ locally. Editing a row of X here means determining which column to place the 1 in. The change made in row i of X only impacts the ith row and ith column of $A - XX^T$. The column to place the 1 in that minimizes the objective locally is:

$$k^* = \underset{k=1,\ldots,K}{\operatorname{argmin}} \|A_i - X_k\|^2 \tag{6.12}$$

where A_i refers to the ith column of A and X_k to the kth column of X. This is because the ith column of XX^T is X_k, where k is the parcel that vertex i has been assigned to.

In the case of incomplete matrix A, the column selection rule in 6.12 should replaced by

$$k^* = \underset{k=1,\ldots,K}{\operatorname{argmin}} \sum_{j \in A_i} (A_{ij} - X_{jk})^2. \tag{6.13}$$

The squared terms in (6.12) and (6.13) can also be changed to absolute value.

Algorithm 5 SymBMF

Initialize $X \in \{0,1\}^{n \times k}$ such that $Xe_k = e_n$
$i \leftarrow 1$
$j \leftarrow 1$
repeat
    $k \leftarrow$ index of 1 entry of x_i
    $x_{ik} \leftarrow 0$
    Compute k^* by (6.12) or (6.13)
    $x_{ik^*} \leftarrow 1$
    if $k \neq k^*$ **then** ▷ row i has been edited
        $j \leftarrow i$
    end if
    $i \leftarrow (i \mod n) + 1$
until $i = j$

The stopping criterion halts the loop before iteration i if no rows have been edited since x_i was last edited.

6.3.2 Mixed Integer Programming Method

The MIP method begins by replacing objective's squared term in the Frobenius norm with an L1 penalty. This new objective function is equivalent to the original if A is binary. Specifically,

$$\begin{array}{lll} \text{minimize} & \sum_{(i,j) \in A} |A_{ij} - x_i^T x_j| & \\ \text{subject to} & x_i \in \{0,1\}^k & \text{for } i = 1, \ldots, n \\ & e_k^T x_i = 1 & \text{for } i = 1, \ldots, n. \end{array}$$

This problem would be a mixed integer program if it were not for the quadratic $x_i^T x_j$ in the objective. We substitute a new variable $y_{ij} = x_i^T x_j$ and find linear constraints that make this relation true for binary x_i satisfying $e_k^T x_i = 1$. Note that an equivalent definition of y_{ij} is

$$y_{ij} = \begin{cases} 1 & \text{if } x_i = x_j \\ 0 & \text{otherwise} \end{cases}$$

The following lemma provides an linearization of $x_i^T x_j$:

Lemma 6.3.1 *Let x_i and x_j both be k-dimensional binary vectors that sum to 1. Then $y_{ij} = x_i^T x_j$ is equivalent to*

$$y_{ij} \leq \min(x_i - x_j) + 1$$

$$y_{ij} \geq \max(x_i + x_j) - 1$$

Proof Follows from the fact that $\min(x_i - x_j) + 1$ and $\max(x_i + x_j) - 1$ both equal 1 if x_i and x_j are equal and 0 if not. ■

Substituting y_{ij} and adding the above linear constraints gives us the following MIP equivalent of SymBMF.

$$\begin{array}{lll} \text{minimize} & \sum_{(i,j)\in A} |A_{ij} - y_{ij}| & \\ \text{subject to} & x_i \in \{0,1\}^k & \text{for } i = 1, ..., n \\ & e_k^T x_i = 1 & \text{for } i = 1, ..., n \\ & \begin{cases} y_{ij} \leq x_{ik} - x_{jk} + 1 \\ y_{ij} \geq x_{ik} + x_{jk} - 1 \end{cases} & \text{for } (i,j) \in A,\ k = 1, ..., K \end{array}$$

To enforce partition connectedness we can add the constraint $(B - I)X \geq 0$ from (6.2.2) where B is the unweighted assignment matrix.

Chapter 7

Mixed Integer and Linear Programming

Need some introductory text. What happened in the previous chapter, what will happen in this chapter?

7.1 A Global Solution to Mean Adjacent Within Edge

We want to find a partitioning of graph $G(V, E)$ into K components so as to minimize the Adjacent-Score (Equation 3.1.2)

$$\frac{1}{K} \sum_{V \in \mathcal{P}_K} \frac{1}{|E_{V,V}|} \sum_{(i,j) \in E_{V,V}} A_{i,j}.$$

Let $m = |E|$, the number of edges in the graph. Assign each edge an index in $\{1, ..., m\}$ and let a be an m-dimensional vector whose jth entry is the weight of the j-indexed edge. Since distance correlation is between 0 and 1, so are the entries of a.

For $k = 1, ..., K$, let $z_k \in \{0, 1\}^m$ be a 0-1 vector with jth entry satisfying

$$z_{jk} = \begin{cases} 1 & \text{if both endpoints of edge } j \text{ are in } V_k \\ 0 & \text{otherwise.} \end{cases}$$

If $z_1, ..., z_K \in \{0, 1\}^m$ describe a valid partitioning, then they must satisfy $\sum_{k=1}^{K} z_{jk} \leq 1$ for all edges j. However, the converse is not true, since this

contraint still allows two edges sharing an endpoint to be within different parcels.

To prevent that from happening, we introduce the assignment matrix $X \in \{0,1\}^{n \times m}$ with entries

$$x_{i,k} = \begin{cases} 1 & \text{if vertex } i \in V_k \\ 0 & \text{otherwise} \end{cases}$$

and three constraints

$$\begin{aligned} 1 + z_{jk} &\geq x_{hk} + x_{ik} \\ z_{jk} &\leq x_{hk} \\ z_{jk} &\leq x_{ik} \end{aligned}$$

for all $j = 1, ..., m$, $k = 1, ..., K$, where (h, i) are the two endpoints of edge j. If we constrain X to be binary then the three above constraints are equivalent to

$$z_{jk} = \begin{cases} 1 & \text{if } x_{hk} = 1 \text{ and } x_{ik} = 1 \\ 0 & \text{otherwise.} \end{cases}$$

For the X, we only need to ensure every vertex is in a parcel and every parcel has at least one vertex (or some other specified minimum):

$$\sum_{k=1}^{K} x_{ik} = 1,$$

$$\sum_{i=1}^{n} x_{ik} \geq 1,$$

where the equation holds for all i and the inequality for all k.

Hence the following optimization problem finds a valid partition that maximizes adjacent-score. This is an instance of generalized fractional linear programming. Let e_m denote a vector of m ones.

$$\text{maximize} \quad \frac{a^T z_1}{e_m^T z_1} + \cdots + \frac{a^T z_K}{e_m^T z_K}$$

$$\text{subject to} \quad \begin{cases} 1 + z_{jk} \geq x_{hk} + x_{ik} \\ z_{jk} \leq x_{hk} \\ z_{jk} \leq x_{ik} \end{cases} \qquad j = 1, ..., m,\ k = 1, ..., K,\ (h, i) = j$$

$$\sum_{j=1}^{m} z_{jk} \geq 1 \qquad k = 1, ..., K$$

$$\sum_{k=1}^{K} x_{ik} = 1 \qquad i = 1, ..., n$$

$$\sum_{i=1}^{n} x_{ik} \geq 1 \qquad k = 1, ..., K$$

$$X \in \{0, 1\}^{n \times K}.$$

Following the result in [Li, 1994] we derive an equivalent Mixed Binary Linear Program to the above. Substitute $y_k = \dfrac{1}{e_m^T z_k}$ for each k, which amounts to introducing a new variable $y \in \mathbb{R}^K$ and non-linear constraints

$$e_m^T z_k y_k = 1$$

The key theorem in [Li, 1994] uses the fact that z_k is binary to linearize this contraint by introducing another variable w_{jk} and using linear constraints to enforce the nonlinear $w_{jk} = z_{jk} y_k$. There are four linear constraints for each w_{jk}:

1. $y_j - w_{jk} \leq 1 - z_{jk}$,
2. $w_{jk} \leq y_j$,
3. $w_{jk} \leq z_{jk}$,
4. $w_{jk} \geq 0$.

If $z_{jk} = 1$, then 1 and 2 will ensure that $w_{jk} = y_k$. If $z_{jk} = 0$, then 3 and 4 will ensure that $w_{jk} = 0$. It is important to note that this construction wouldn't work if $y_k > 1$. In our case, this occurs if and only if $z_{jk} = 0$ for all j, which has already been excluded by the $\sum_{j=1}^{m} z_{jk} \geq 1$ constraint.

Now we are ready to present the mixed integer version

$$
\begin{array}{ll}
\text{maximize} & a^T w_1 + \cdots + a^T w_K \\
\text{subject to} & \begin{cases} 1 + z_{jk} \geq x_{hk} + x_{ik} \\ z_{jk} \leq x_{hk} \\ z_{jk} \leq x_{ik} \end{cases} \qquad j = 1, ..., m,\ k = 1, ..., K,\ (h, i) = j \\
& \sum_{j=1}^{m} z_{jk} \geq 1 \qquad k = 1, ..., K \\
& \sum_{k=1}^{K} x_{ik} = 1 \qquad i = 1, ..., n \\
& \sum_{i=1}^{n} x_{ik} \geq 1 \qquad k = 1, ..., K \\
& X \in \{0, 1\}^{n \times K} \\
& \sum_{j=1}^{m} w_{jk} = 1 \qquad k = 1, ..., K \\
& \begin{cases} y_j - w_{jk} \leq 1 - z_{jk} \\ w_{jk} \leq y_j \\ w_{jk} \leq z_{jk} \\ w_{jk} \geq 0 \end{cases} \qquad j = 1, ..., m,\ k = 1, ..., K.
\end{array}
$$

which can be solved globally by branch-and-bound methods. Unfortunately the size of our graph is too large for a generic MIP solver, and the largest graphs we partitioned using this method had around 400 vertices and 3000 edges, partitioned into 10 components. This is true even when the binary $\{0, 1\}$ constraint was relaxed to an interval $[0, 1]$ to create an LP.

7.2 An Approximate Solution Using SymBMF

A faster approximation with fewer variables to this MIP involves dropping the assignment matrix X. The problem becomes

$$
\begin{array}{lll}
\text{maximize} & \dfrac{a^T z_1}{e_m^T z_1} + \cdots + \dfrac{a^T z_K}{e_m^T z_K} & \\
\text{subject to} & \sum_{k=1}^{K} z_k = e_m & \\
& e_m^T z_k \geq 1 & \text{for } k = 1, ..., K \\
& z_k \in \{0, 1\}^m & \text{for } k = 1, ..., K.
\end{array}
$$

Using the [Li, 1994] transformation mentioned above, we get

$$
\begin{aligned}
\text{maximize} \quad & a^T w_1 + \cdots + a^T w_K \\
\text{subject to} \quad & \textstyle\sum_{k=1}^{K} z_k = e_m \\
& e_m^T z_k \geq 1 && \text{for } k = 1, ..., K \\
& z_k \in \{0,1\}^m && \text{for } k = 1, ..., K \\
& \textstyle\sum_{j=1}^{m} w_{jk} = 1 && k = 1, ..., K \\
& \begin{cases} y_j - w_{jk} \leq 1 - z_{jk} \\ w_{jk} \leq y_j \\ w_{jk} \leq z_{jk} \\ w_{jk} \geq 0 \end{cases} && j = 1, ..., m,\ k = 1, ..., K.
\end{aligned}
$$

If $K > 1$ and the graph is connected, then not every edge can be within a parcel; there must be at least one that is between two different parcels. However, the first constraint $\sum_{k=1}^{K} z_k = e_m$ forces the contrary — every edge must be assigned to exactly one parcel. Why does this constraint have to be an equality rather than a $\leq$ as in the first MIP? If it were the latter the optimal solution to this problem would be trivial: take the K edges with the largest weights in the graph and assign each to a different parcel. Do not assign any other entries of z_k 1. This optimal solution is useless for partitioning. This is a consequence of eliminating the X matrix from the first problem.

If the edges of the graph are over-assigned by z_k, how do we recover the assignment matrix X? We propose to create an approximate partition matrix (5.2.2) P from the z_k so that

$$
P_{ij} = \begin{cases} 1 & \text{if } \underset{k}{\text{argmax}}\ z_{ik} = \underset{k}{\text{argmax}}\ z_{jk} \\ 0 & \text{otherwise.} \end{cases}
$$

Following this we could use either of the SymBMF methods introduced in the previous chapter to find a decomposition $P \approx XX^T$.

For this method (and others), also mention the implementation. What language and what packages?

Chapter 8

Results

Some lead into here.

8.1 Summary of Methods

Table (8.1) summarizes the objectives, advantages, and drawbacks of each partitioning method we've presented in the previous chapters. Clearly, the requirement of parcels to be connected components is the biggest roadblock to developing a good method.

There is a post-processing method that can take a parcellation with disconnected components and modify it to be connected. The method is to treat each separate component of a parcel as new parcels, create a Contractible Graph with these new parcels as components, and apply the (Generalized)

Table 8.1: Summary of Partitioning Methods

Section	Objective	Method	Optimality	Fast	Connected	Balanced	Smooth
4.1	MaxAWE	Add-Edge	Approx	Yes	Yes	No	No
4.2	MaxAWE	Edge-Contract	Approx	Yes	Yes	Yes	No
4.3	MaxAWE	Generalized EC	Approx	Yes	Yes	Yes	Yes
5.2	Min Ratio-Cut	Spectral	Approx	Yes	Mostly	Yes	Yes
6.1	SymNMF	ANLS	Approx	No	No	Yes	Yes
6.3.1	SymBMF	C Switching	Approx	Yes	No	Yes	No
6.3.2	SymBMF	MIP	Global	No	No	Yes	No
7.1	MaxAWE	MIP	Global	No	No	Yes	No
7.2	MaxAWE	MIP	Approx	No	No	Yes	No

Edge Contract algorithm. This was carried out as a post-processing step in the spectral and SymBMF parcellations, detailed in the next section.

The second limiting factor is computational time. The Alternating Non-negative Least Squares algorithm can be made to work on graphs as large as the brain, but this would require some specialized data structures for the computation of X and Y to avoid re-computing unchanged columns. Unfortunately we did not have enough time to implement this.

The problem of computational time is most evident in the integer (and linear) programming methods. The fact that our brain data was too large for even the lightest linear program shows that this generic optimization approach is typically not feasible. However, these proposed methods may be of use to problems with smaller data sets.

One possible approach to dealing with computational time that we have not had the time to explore is to apply the MIP methods to small subgraphs of the brain. For instance, one could take the AAL parcellation and obtain a finer parcellation by using a MIP method on each of the AAL parcels.

The only method that satisfies the requirements of computational speed, parcel connectedness, size balance, and smoothness without any post-processing steps is the Generalized Edge-Contraction family of algorithms. In the next section we will show that it is also the parcellation method that produces the best Adjacent-Scores.

All of the methods above can be applied to the similar problem of *clustering*. In fact, similarity-based clustering is just a special case of graph partitioning where the graph is fully connected (i.e., every vertex has an edge to every other vertex), so connectedness of partitions is no longer a relevant factor. Then, if we define the Adjacent-Score in terms of similarity equal to negative Euclidean distance squared

$$\frac{1}{K}\sum_{k=1}^{K}\frac{1}{\binom{|V_k|}{2}}\sum_{x,y\in V_k}-\|x-y\|^2,$$

the objective of maximizing Adjacent-Score becomes equivalent to minimizing a weighted within-cluster sum of squares objective

$$\sum_{k=1}^{K}\frac{1}{\binom{|V_k|}{2}}\sum_{x\in V_k}\|x-\mu_k\|^2$$

where μ_k is the mean of all x in V_k.

It'll be nice to cite the equations in Chapter 3 for the criterion values

Table 8.2: Criteria Scores of Various Parcellation Methods, Averaged Across Normal Brains

	Adjacent	Boundary	RatioCut	CompParc	Balance	Jaggedness
AAL	0.747	0.804	74.735	1.375	0.324	28.791
GenEC (3,1)	0.766	0.799	47.118	1	0.251	23.930
GenEC (6,1)	0.774	0.796	51.342	1	0.280	28.801
GenEC (6,4)	0.773	0.800	51.285	1	0.335	29.199
Spectral	0.747	0.810	43.242	1.027	0.728	16.347
Spectral GenEC(6,4)	0.747	0.810	43.162	1	0.713	16.305
SymBMF	0.845	0.962	293.662	470.994	0.838	305.302
SymBMF GenEC(6,4)	0.773	0.798	53.256	1	0.290	30.086

8.2 Parcellations of ABIDE fMRI Scans

Tables (8.2) and (8.3) respectively show the results of various parcellation methods carried out on resting state fMRI scans of 6 control and 6 autism patients. The number of parcels in each method is set to 116, the same as AAL. Each brain was preprocessed to remove vertices with edge weights of 0 to all adjacent vertices. For each method and criterion, the values are averaged over the six subjects in each cohort. In our methods, SymBMF was carried out using component switching on the incomplete adjacency matrix (only approximation of non-zero entries in the A matrix was considered). GenEC (α, β) denotes a Generalized Edge-Contract algorithm using standard priority function (4.1) with parameters α and β. When this is written after a different method such as Spectral, it means we post-processed the Spectral parcellation using GenEC to obtain connected parcels.

Despite producing a parcellation with the highest Adjacent-Score, the Component Switching SymBMF method is the least suitable for parcellation since its parcels are extremely fragmented, with an average 473 components per parcel. The reason for this is that the adjacency matrix was treated as incomplete, so there was no penalty for a vertex belonging to a parcel with many vertices it is disconnected from. The high Adjacent-Score of SymBMF parcellations suggests a trade-off between maximizing weights of within edges and creating connected and smooth parcels.

Table 8.3: Criteria Scores of Various Parcellation Methods, Averaged Across Autism Spectrum Brains

	Adjacent	Boundary	RatioCut	CompParc	Balance	Jaggedness
AAL	0.735	0.821	74.675	1.365	0.323	28.882
GenEC (3,1)	0.762	0.821	46.615	1	0.210	25.008
GenEC (6,1)	0.769	0.827	51.613	1	0.249	31.178
GenEC (6,4)	0.771	0.821	51.705	1	0.309	31.821
Spectral	0.739	0.827	42.464	1.024	0.697	16.360
Spectral GenEC(6,4)	0.739	0.827	42.427	1	0.677	16.333
SymBMF	0.844	0.969	289.129	473.102	0.827	306.992
SymBMF GenEC(6,4)	0.769	0.821	52.742	1	0.261	31.927

The other parcellations aside from pure SymBMF has CompParc, Balance, and Jaggedness scores that were at least as good as the AAL ones. The Spectral parcellations were the smoothest, as expected, but this came at the cost of lower Adjacent-Score and higher Boundary-Score relative to the GenEC parcellations. In both groups, the Generalized Edge-Contract with parameters $\alpha = 6$ and $\beta = 4$ performed best. These parcellations had the highest Adjacent-Scores and while maintaining Balance and Jaggedness Scores close to those of the AAL. There is no significant difference in the parcellation results of autism and control brains.

8.3 Reproducibility of Parcellations and Cross-Validation

We measured the similarity of 116-parcel parcellations from different methods on the same brain, across brains in the control and autistic cohorts. We used the Adjusted Rand Index **??** Citation doesn't work as our measure of similarity, where 1 means identical parcel assignments and 0 means no different from random parcel assignments. The result is shown in Figure (8.1). The last row and column refer to ARI values with respect to a random parcellation, generated by applying GenEC (6,4) to the same brain graph with edge weights shuffled. The reason for this is to account for the portion

Figure 8.1: Adjusted Rand Index Between Different 116-Parcel Parcellations of the same fMRI Scan, Averaged over All Subjects

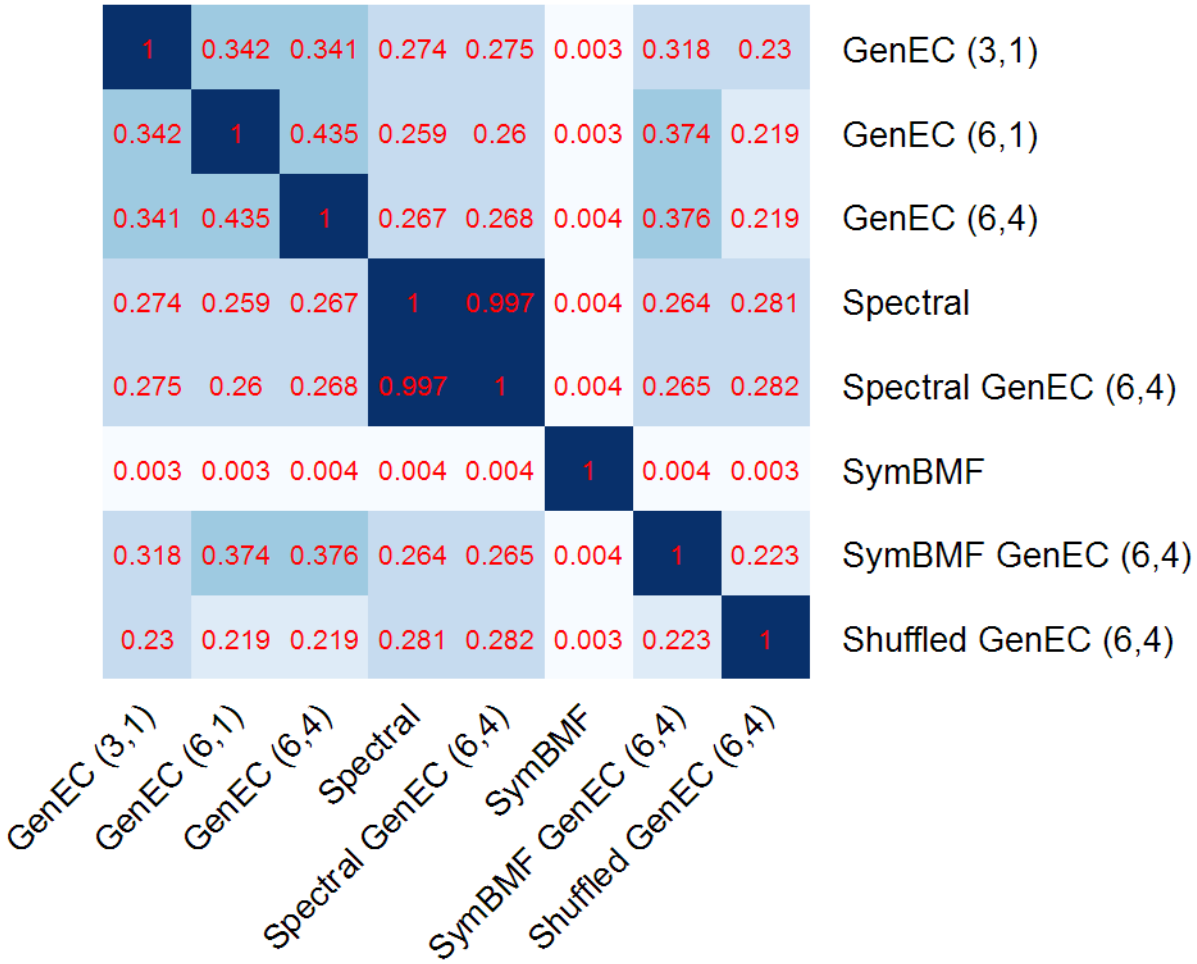

Figure 8.2: Adjusted Rand Index Between 116-Parcel GenEC(6,4) Parcellations on Different fMRI Scans

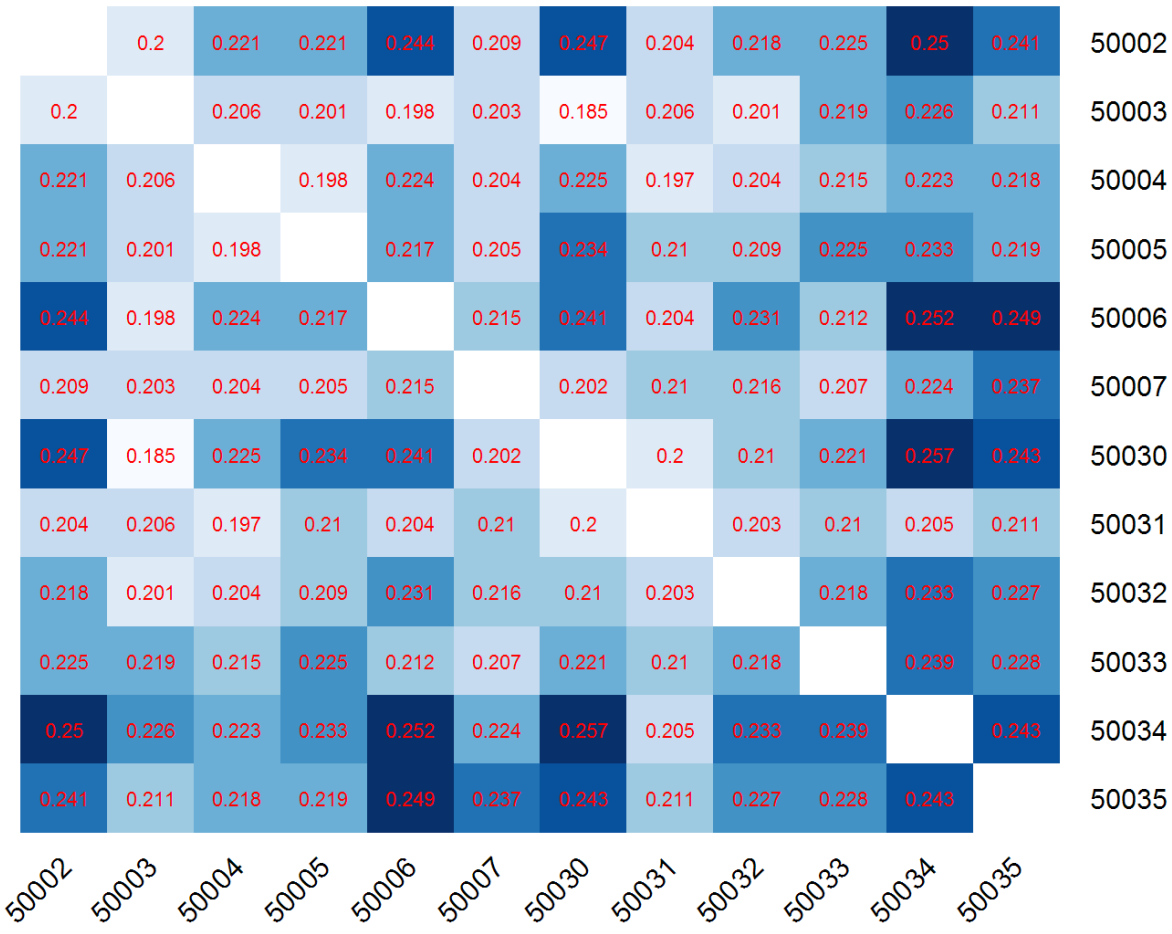

of ARI scores that derive solely from the connectedness and smoothness property of parcellations.

As expected, the first three GenEC parcellations are similar to one another, more than they are to the shuffled parcellation or to the Spectral parcellations. The SymBMF GenEC (6,4) parcellation can also be grouped with the first three. The unconnected SymBMF parcellation is similar to no other since it is too fragmented.

Next, we restricted ourselves to the GenEC (6,4) method and measured how similar the parcellations this method produced on different brains are. The results are shown in Figure (8.2). From Figure (8.1) we know that the ARI between a GenEC (6,4) parcellation on a shuffled brain graph and an actual one is around 0.219. Surprisingly, for nearly all pairs of brains, the ARI value between their GenEC (6,4) parcellations is no greater than this. We also see that the mean ARI between autistic and control brains is not significantly different from the mean ARI between brains of the same cohort at the 116-parcel level. This suggests too much variation in the spatial distribution of distance correlations across the edges of different brain graphs for there to be a common parcellation fitting all brains.

To verify this, we conducted a cross-validation procedure where for each pair of brains, we let one be the parcellation brain and one be the validation brain. On the parcellation brain we performed two parcellations: GenEC (6,4) and Shuffled GenEC (6,4) for the control. On the validation brain we computed the Adjacent-Scores of both parcellations. We stored the difference GenEC minus Shuffled in a 12 by 12 matrix, displayed in Figure (8.3). The diagonal values are in-sample Adjacent-Scores where the parcellation brain and the validation brain are the same.

Assuming normality, a one sample t-test of the mean non-diagonal cross-validation value shows that it is significantly greater than 0 ($p \leq 2.2 \times 10^{-16}$). This indicates some degree of similarity between different brains in the statistical dependencies of adjacent voxels. Furthermore, Welch's two sample t-test of unequal variances tells us the mean off-diagonal CV value in the autism cohort and the control cohort are unequal ($p = 0.0138$). The control group has a higher realized mean. These observations can serve as a basis for further study.

Finally, we investigate whether the GenEC (6,4) parcellations could be overfitting. The GenEC methods produced parcellations that scored well in-sample (diagonal mean 0.048) but not as well out-of-sample (off-diagonal mean 0.010), so it is possible that the parcellations they produce are too

Figure 8.3: Difference of Adjacent-Score, Cross-Validation of 116-Parcel GenEC (6,4) Parcellation on 12 Autism and Control Brains

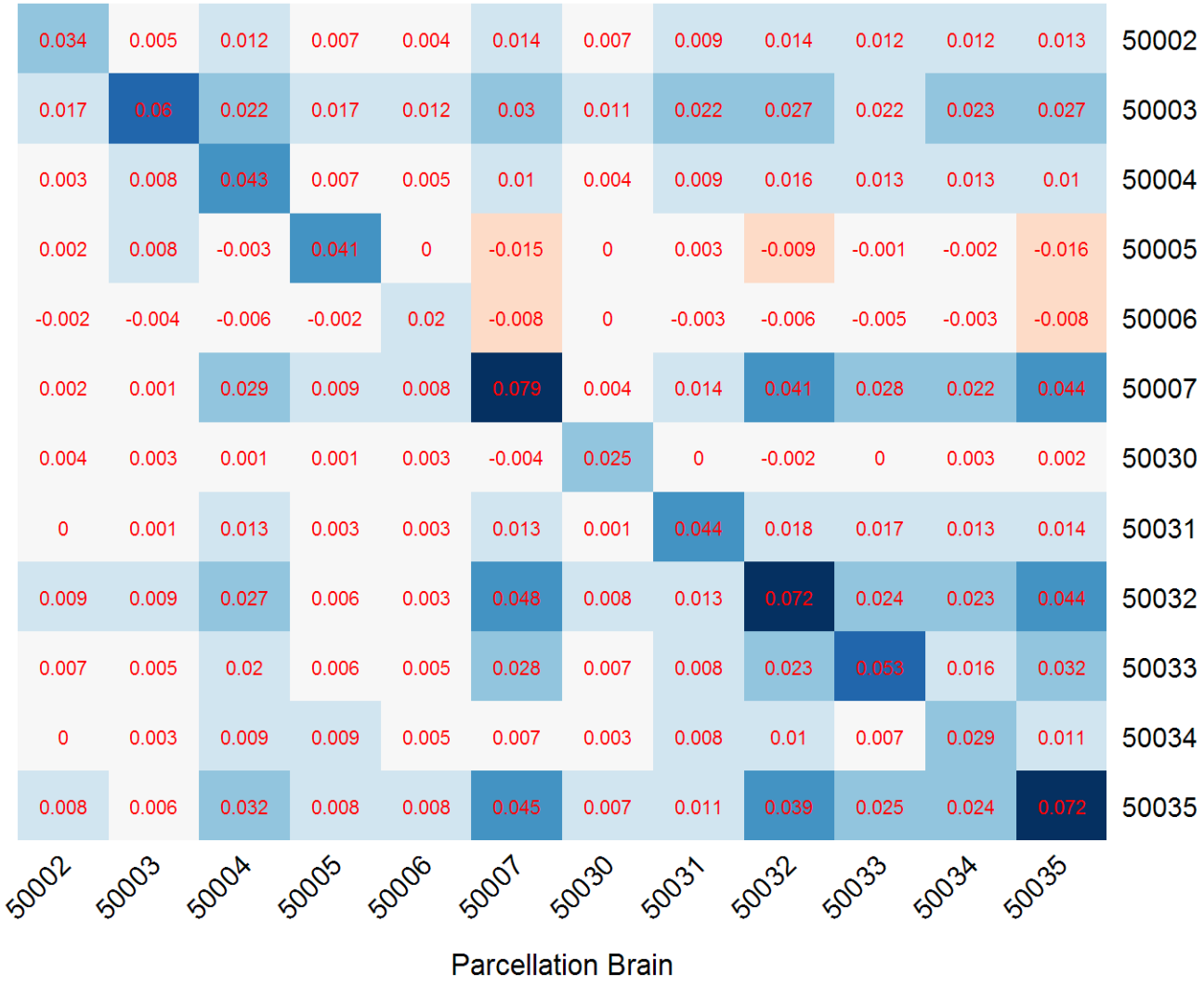

flexible. To see if this could be the case, we perform the same cross-validation procedure except now using the spectral method. The reason for this is that partitions obtained via the spectral method have lower Jaggedness values and smoother surfaces, and hence are less likely to overfit the graph.

Figure (8.4) shows the results of the cross-validation procedure using the spectral partitioning method.

8.4 Conclusion

Some things to think about: Future Work, general thoughts about parcellation, which methods did you expect to do well and which actually did well.

Figure 8.4: Difference of Adjacent-Score, Cross-Validation of 116-Parcel Spectral Parcellation on 12 Autism and Control Brains

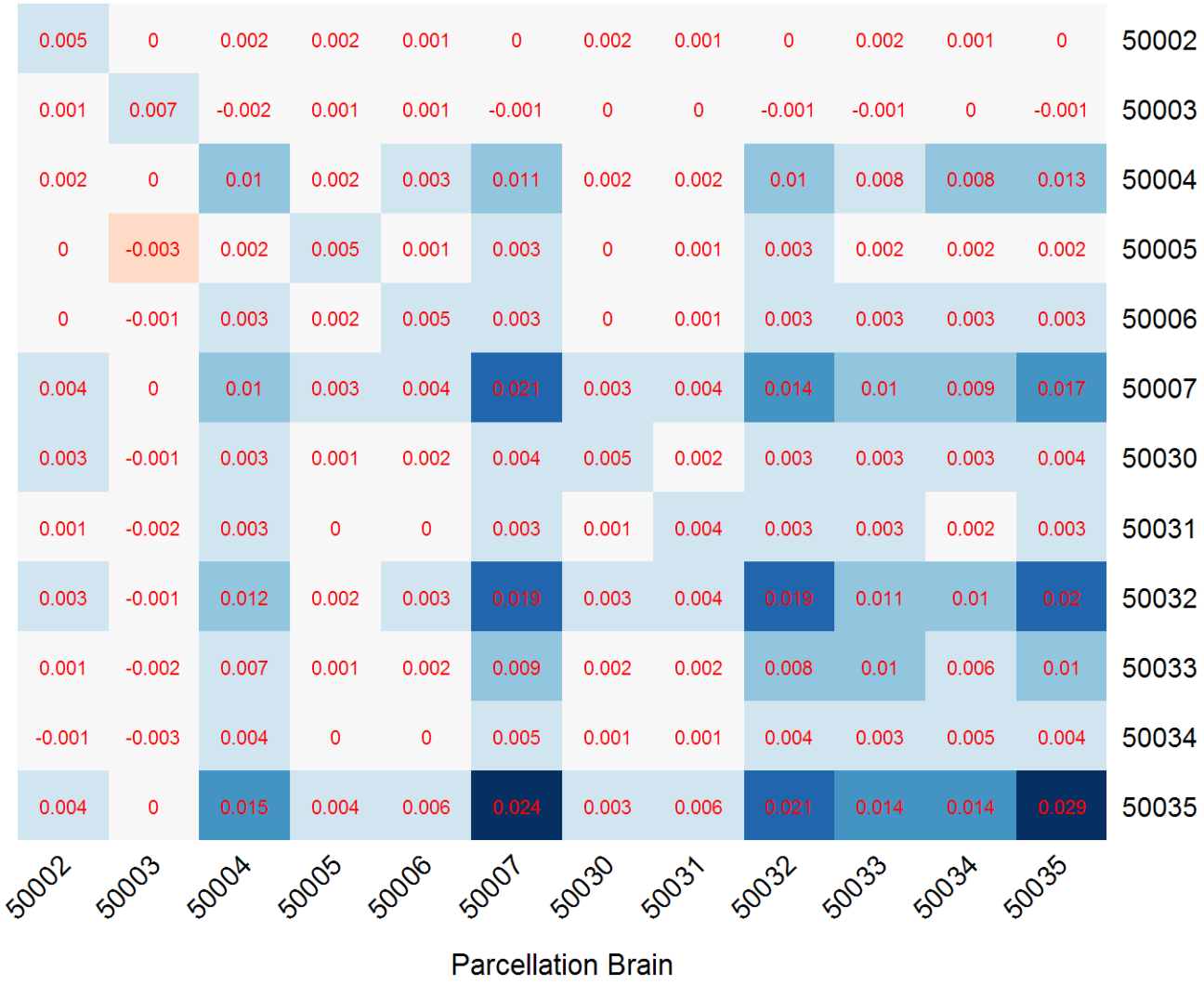

Bibliography

[Alexander-Bloch et al., 2012] Alexander-Bloch, A., Lambiotte, R., Roberts, B., Giedd, J., Gogtay, N., and Bullmore, E. (2012). The discovery of population differences in network community structure: new methods and applications to brain functional networks in schizophrenia. *Neuroimage*, 59(4):3889–3900.

[Barnes et al., 2011] Barnes, K. A., Nelson, S. M., Cohen, A. L., Power, J. D., Coalson, R. S., Miezin, F. M., Vogel, A. C., Dubis, J. W., Church, J. A., Petersen, S. E., et al. (2011). Parcellation in left lateral parietal cortex is similar in adults and children. *Cerebral Cortex*, page bhr189.

[Beckmann et al., 2005] Beckmann, C. F., DeLuca, M., Devlin, J. T., and Smith, S. M. (2005). Investigations into resting-state connectivity using independent component analysis. *Philosophical Transactions of the Royal Society of London B: Biological Sciences*, 360(1457):1001–1013.

[Bellec et al., 2006] Bellec, P., Perlbarg, V., Jbabdi, S., Pélégrini-Issac, M., Anton, J.-L., Doyon, J., and Benali, H. (2006). Identification of large-scale networks in the brain using fmri. *Neuroimage*, 29(4):1231–1243.

[Biswal et al., 2010] Biswal, B. B., Mennes, M., Zuo, X.-N., Gohel, S., Kelly, C., Smith, S. M., Beckmann, C. F., Adelstein, J. S., Buckner, R. L., Colcombe, S., et al. (2010). Toward discovery science of human brain function. *Proceedings of the National Academy of Sciences*, 107(10):4734–4739.

[Blumensath et al., 2013] Blumensath, T., Jbabdi, S., Glasser, M. F., Van Essen, D. C., Ugurbil, K., Behrens, T. E., and Smith, S. M. (2013). Spatially constrained hierarchical parcellation of the brain with resting-state fmri. *Neuroimage*, 76:313–324.

[Buluç et al., 2013] Buluç, A., Meyerhenke, H., Safro, I., Sanders, P., and Schulz, C. (2013). Recent advances in graph partitioning. *CoRR*, abs/1311.3144.

[Centers for Disease Control, 2010] Centers for Disease Control (2010). Autism and developmental disabilities monitoring (ADDM) network. *Technical Report*, 19.

[Chan et al., 1994] Chan, P. K., Schlag, M. D., and Zien, J. Y. (1994). Spectral k-way ratio-cut partitioning and clustering. *Computer-Aided Design of Integrated Circuits and Systems, IEEE Transactions on*, 13(9):1088–1096.

[Chen et al., 2008] Chen, S., Ross, T. J., Zhan, W., Myers, C. S., Chuang, K.-S., Heishman, S. J., Stein, E. A., and Yang, Y. (2008). Group independent component analysis reveals consistent resting-state networks across multiple sessions. *Brain research*, 1239:141–151.

[Cohen et al., 2008] Cohen, A. L., Fair, D. A., Dosenbach, N. U., Miezin, F. M., Dierker, D., Van Essen, D. C., Schlaggar, B. L., and Petersen, S. E. (2008). Defining functional areas in individual human brains using resting functional connectivity mri. *Neuroimage*, 41(1):45–57.

[Collins et al., 1994] Collins, D. L., Neelin, P., Peters, T. M., and Evans, A. C. (1994). Automatic 3d intersubject registration of mr volumetric data in standardized talairach space. *Journal of computer assisted tomography*, 18(2):192–205.

[Craddock et al., 2012] Craddock, R. C., James, G. A., Holtzheimer, P. E., Hu, X. P., and Mayberg, H. S. (2012). A whole brain fmri atlas generated via spatially constrained spectral clustering. *Human brain mapping*, 33(8):1914–1928.

[De Luca et al., 2006] De Luca, M., Beckmann, C., De Stefano, N., Matthews, P., and Smith, S. M. (2006). fmri resting state networks define distinct modes of long-distance interactions in the human brain. *Neuroimage*, 29(4):1359–1367.

[Diez et al., 2014] Diez, I., Bonifazi, P., Escudero, I., Mateos, B., Muñoz, M. A., Stramaglia, S., and Cortes, J. M. (2014). A novel brain partition highlights the modular skeleton shared by structure and function. *arXiv preprint arXiv:1410.7959*.

[Ding et al., 2005] Ding, C. H., He, X., and Simon, H. D. (2005). On the equivalence of nonnegative matrix factorization and spectral clustering. In *SDM*, volume 5, pages 606–610. SIAM.

[Evans et al., 1993] Evans, A. C., Collins, D. L., Mills, S., Brown, E., Kelly, R., and Peters, T. M. (1993). 3d statistical neuroanatomical models from 305 mri volumes. In *Nuclear Science Symposium and Medical Imaging Conference, 1993., 1993 IEEE Conference Record.*, pages 1813–1817. IEEE.

[Fan, 1950] Fan, K. (1950). On a theorem of weyl concerning eigenvalues of linear transformations ii. *Proceedings of the National Academy of Sciences*, 36(1):31–35.

[Flandin et al., 2002] Flandin, G., Kherif, F., Pennec, X., Rivière, D., Ayache, N., and Poline, J.-B. (2002). Parcellation of brain images with anatomical and functional constraints for fmri data analysis. In *Biomedical Imaging, 2002. Proceedings. 2002 IEEE International Symposium on*, pages 907–910. IEEE.

[Goldschmidt and Hochbaum, 1994] Goldschmidt, O. and Hochbaum, D. S. (1994). A polynomial algorithm for the k-cut problem for fixed k. *Mathematics of operations research*, 19(1):24–37.

[Gordon et al., 2014] Gordon, E. M., Laumann, T. O., Adeyemo, B., Huckins, J. F., Kelley, W. M., and Petersen, S. E. (2014). Generation and evaluation of a cortical area parcellation from resting-state correlations. *Cerebral Cortex*, page bhu239.

[Hartman et al., 2011] Hartman, D., Hlinka, J., Paluš, M., Mantini, D., and Corbetta, M. (2011). The role of nonlinearity in computing graph-theoretical properties of resting-state functional magnetic resonance imaging brain networks. *Chaos: An Interdisciplinary Journal of Nonlinear Science*, 21(1):013119.

[He et al., 2009] He, Y., Wang, J., Wang, L., Chen, Z. J., Yan, C., Yang, H., Tang, H., Zhu, C., Gong, Q., Zang, Y., et al. (2009). Uncovering intrinsic modular organization of spontaneous brain activity in humans. *PloS one*, 4(4):e5226.

[Heller et al., 2006] Heller, R., Stanley, D., Yekutieli, D., Rubin, N., and Benjamini, Y. (2006). Cluster-based analysis of fmri data. *NeuroImage*, 33(2):599–608.

[Kim and Park, 2011] Kim, J. and Park, H. (2011). Fast nonnegative matrix factorization: An active-set-like method and comparisons. *SIAM Journal on Scientific Computing*, 33(6):3261–3281.

[Kuang et al., 2015] Kuang, D., Yun, S., and Park, H. (2015). Symnmf: nonnegative low-rank approximation of a similarity matrix for graph clustering. *Journal of Global Optimization*, 62(3):545–574.

[Li, 1994] Li, H.-L. (1994). A global approach for general 0–1 fractional programming. *European Journal of Operational Research*, 73(3):590–596.

[Liu et al., 2008] Liu, Y., Liang, M., Zhou, Y., He, Y., Hao, Y., Song, M., Yu, C., Liu, H., Liu, Z., and Jiang, T. (2008). Disrupted small-world networks in schizophrenia. *Brain*, 131(4):945–961.

[Lord et al., 2000] Lord, C., Risi, S., Lambrecht, L., Cook Jr, E. H., Leventhal, B. L., DiLavore, P. C., Pickles, A., and Rutter, M. (2000). The autism diagnostic observation schedulegeneric: A standard measure of social and communication deficits associated with the spectrum of autism. *Journal of autism and developmental disorders*, 30(3):205–223.

[Lord et al., 1994] Lord, C., Rutter, M., and Le Couteur, A. (1994). Autism diagnostic interview-revised: a revised version of a diagnostic interview for caregivers of individuals with possible pervasive developmental disorders. *Journal of autism and developmental disorders*, 24(5):659–685.

[Lu et al., 2003] Lu, Y., Jiang, T., and Zang, Y. (2003). Region growing method for the analysis of functional mri data. *NeuroImage*, 20(1):455–465.

[Lynall et al., 2010] Lynall, M.-E., Bassett, D. S., Kerwin, R., McKenna, P. J., Kitzbichler, M., Muller, U., and Bullmore, E. (2010). Functional connectivity and brain networks in schizophrenia. *The Journal of Neuroscience*, 30(28):9477–9487.

[Mezer et al., 2009] Mezer, A., Yovel, Y., Pasternak, O., Gorfine, T., and Assaf, Y. (2009). Cluster analysis of resting-state fmri time series. *Neuroimage*, 45(4):1117–1125.

[Newman, 2006] Newman, M. E. (2006). Modularity and community structure in networks. *Proceedings of the National Academy of Sciences*, 103(23):8577–8582.

[Peltier et al., 2003] Peltier, S. J., Polk, T. A., and Noll, D. C. (2003). Detecting low-frequency functional connectivity in fmri using a self-organizing map (som) algorithm. *Human brain mapping*, 20(4):220–226.

[Power et al., 2011] Power, J. D., Cohen, A. L., Nelson, S. M., Wig, G. S., Barnes, K. A., Church, J. A., Vogel, A. C., Laumann, T. O., Miezin, F. M., Schlaggar, B. L., et al. (2011). Functional network organization of the human brain. *Neuron*, 72(4):665–678.

[Ryali et al., 2013] Ryali, S., Chen, T., Supekar, K., and Menon, V. (2013). A parcellation scheme based on von mises-fisher distributions and markov random fields for segmenting brain regions using resting-state fmri. *NeuroImage*, 65:83–96.

[Salvador et al., 2005] Salvador, R., Suckling, J., Coleman, M. R., Pickard, J. D., Menon, D., and Bullmore, E. (2005). Neurophysiological architecture of functional magnetic resonance images of human brain. *Cerebral cortex*, 15(9):1332–1342.

[Sejdinovic et al., 2013] Sejdinovic, D., Sriperumbudur, B., Gretton, A., Fukumizu, K., et al. (2013). Equivalence of distance-based and rkhs-based statistics in hypothesis testing. *The Annals of Statistics*, 41(5):2263–2291.

[Shen et al., 2010] Shen, X., Papademetris, X., and Constable, R. T. (2010). Graph-theory based parcellation of functional subunits in the brain from resting-state fmri data. *Neuroimage*, 50(3):1027–1035.

[Shen et al., 2013] Shen, X., Tokoglu, F., Papademetris, X., and Constable, R. T. (2013). Groupwise whole-brain parcellation from resting-state fmri data for network node identification. *Neuroimage*, 82:403–415.

[Smith et al., 2009] Smith, S. M., Fox, P. T., Miller, K. L., Glahn, D. C., Fox, P. M., Mackay, C. E., Filippini, N., Watkins, K. E., Toro, R., Laird, A. R.,

et al. (2009). Correspondence of the brain's functional architecture during activation and rest. *Proceedings of the National Academy of Sciences*, 106(31):13040–13045.

[Spoormaker et al., 2010] Spoormaker, V. I., Schröter, M. S., Gleiser, P. M., Andrade, K. C., Dresler, M., Wehrle, R., Sämann, P. G., and Czisch, M. (2010). Development of a large-scale functional brain network during human non-rapid eye movement sleep. *The Journal of neuroscience*, 30(34):11379–11387.

[Supekar et al., 2008] Supekar, K., Menon, V., Rubin, D., Musen, M., Greicius, M. D., et al. (2008). Network analysis of intrinsic functional brain connectivity in alzheimers disease. *PLoS Comput Biol*, 4(6):e1000100.

[Székely, 2003] Székely, G. (2003). E-statistics: The energy of statistical samples. *Bowling Green State University, Department of Mathematics and Statistics Technical Report*, (03-05):2000–2003.

[Székely and Rizzo, 2013] Székely, G. J. and Rizzo, M. L. (2013). Energy statistics: A class of statistics based on distances. *Journal of statistical planning and inference*, 143(8):1249–1272.

[Székely et al., 2007] Székely, G. J., Rizzo, M. L., Bakirov, N. K., et al. (2007). Measuring and testing dependence by correlation of distances. *The Annals of Statistics*, 35(6):2769–2794.

[Thirion et al., 2006] Thirion, B., Flandin, G., Pinel, P., Roche, A., Ciuciu, P., and Poline, J.-B. (2006). Dealing with the shortcomings of spatial normalization: Multi-subject parcellation of fmri datasets. *Human brain mapping*, 27(8):678–693.

[Tian et al., 2011] Tian, L., Wang, J., Yan, C., and He, Y. (2011). Hemisphere-and gender-related differences in small-world brain networks: a resting-state functional mri study. *Neuroimage*, 54(1):191–202.

[Tzourio-Mazoyer et al., 2002] Tzourio-Mazoyer, N., Landeau, B., Papathanassiou, D., Crivello, F., Etard, O., Delcroix, N., Mazoyer, B., and Joliot, M. (2002). Automated anatomical labeling of activations in spm using a macroscopic anatomical parcellation of the mni mri single-subject brain. *Neuroimage*, 15(1):273–289.

[Van Den Heuvel et al., 2008] Van Den Heuvel, M., Mandl, R., and Hulshoff Pol, H. (2008). Normalized cut group clustering of resting-state fmri data. *PloS one*, 3(4):e2001.

[Wang et al., 2009] Wang, J., Wang, L., Zang, Y., Yang, H., Tang, H., Gong, Q., Chen, Z., Zhu, C., and He, Y. (2009). Parcellation-dependent small-world brain functional networks: A resting-state fmri study. *Human brain mapping*, 30(5):1511–1523.

[Zhang et al., 2014] Zhang, Y., Caspers, S., Fan, L., Fan, Y., Song, M., Liu, C., Mo, Y., Roski, C., Eickhoff, S., Amunts, K., and Jiang, T. (2014). Robust brain parcellation using sparse representation on resting-state fmri. *Brain Structure and Function*, pages 1–15.